frontiers in Earth Science

ORIGINAL RESEARCH
published: 11 October 2021
doi: 10.3389/feart.2021.731233

Genesis of High-Mg Adakites in the Southeastern Margin of North China Craton: Geochemical and U-Pb Geochronological Perspectives

Shuo Zheng[1,2], Yanfei An[1]*, Chunkit Lai[3], Hongzhi Wang[4] and Yunfeng Li[4]

[1]School of Resources and Environment Engineering, Anhui University, Hefei, China, [2]Exploration Research Institute, Anhui Provincial Bureau of Coal Geology, Hefei, China, [3]Faculty of Science, University of Brunei Darussalam, Bandar Seri Begawan, Brunei, [4]Third Exploration Team of Anhui Provincial Bureau of Coal Geology, Suzhou, China

Edited by:
Hassan Mirnejad,
Miami University, United States

Reviewed by:
Wayne Powell,
Brooklyn College (CUNY),
United States
Mohsen Rezaei,
Shahid Chamran University of
Ahvaz, Iran

***Correspondence:**
Yanfei An
any@ahu.edu.cn

Specialty section:
This article was submitted to
Economic Geology,
a section of the journal
Frontiers in Earth Science

Received: 26 June 2021
Accepted: 21 September 2021
Published: 11 October 2021

Citation:
Zheng S, An Y, Lai C, Wang H and Li Y (2021) Genesis of High-Mg Adakites in the Southeastern Margin of North China Craton: Geochemical and U-Pb Geochronological Perspectives. Front. Earth Sci. 9:731233. doi: 10.3389/feart.2021.731233

In the eastern North China Craton (NCC), Mesozoic tectonics was dominated by the Paleo-Pacific subduction rollback and the Tanlu crustal-scale fault movement. The regional transtension had generated extensive adakitic magmatism, some Cu-Au ore-forming but others not. To establish the geodynamic setting and any metallogenic link for the adakites from the southeastern NCC margin, we analyzed the ore-barren adakitic rocks from underground mines in the Huaibei-Linhuan coalfield (where surface igneous outcrops are scarce), and compared their ages and geochemistry with other mineralized and ore-barren adakites across Eastern China. Zircon U-Pb dating reveals two magmatic episodes in the Huaibei-Linhuan coalfield: 1) early-Early Cretaceous (ca. 130–129 Ma) (quartz-)diorite and granodiorite, and 2) late-Early Cretaceous (ca. 115.8 and 105.8 Ma) microgabbro and dolerite. Whole-rock geochemistry indicates that the (quartz-)diorite and granodiorite are high-Mg adakitic, featured by low K_2O/Na_2O (avg. 0.33), high Sr/La (avg. 44.3), and lack of correlation between SiO_2 (fractionation index) and Sr/Y (avg. 56.55) and MREE/HREE (avg. 1.09), resembling typical adakites derived from oceanic-slab partial melting. Geochronological correlation with the regional tectonic events suggests that the slab-melting may have been caused by the Paleo-Pacific subduction rollback. Further extension and crustal thinning in the late-Early Cretaceous along the southern Tanlu fault may have formed the gabbro-dolerite in the coalfield. Geochemical comparison suggests that parental magma of the Huaibei-Linhuan adakites may have had similar water content [similar zircon 10,000*(Eu/Eu*)/Y and Eu/Eu* ratios] to typical porphyry Cu-Au ore-forming magmas, yet the former may have been considerably more reduced (lower zircon Ce/Nd and whole-rock V/Sc ratios). We considered that the assimilation of Carboniferous-Permian coal seams in the area may have further lowered the magma fO_2 and thus its potential to form Cu-Au mineralization.

Keywords: high-Mg adakites, North China Craton, Paleo-Pacific subduction, Cretaceous, zircon U-Pb dating

INTRODUCTION

The Mesozoic eastern North China craton (NCC) is tectonically complex due to the co-influence of a number of tectonic events, including the North China-South China collision, the Paleo-Pacific subduction and rollback, the gradual NCC decratonization, together with the ~500-km sinistral movement of the regional Tanlu fault zone and the accompanied pull-apart basin formation (e.g., Li et al., 2012, 2017; Hong et al., 2020; Zhang et al., 2020; Sun et al., 2021; Ye et al., 2021). The complex tectonic interactions resulted in the formation of important Cu-Au mineralization across the region, notably the world-class Jiaodong-Liaodong orogenic gold province (e.g., Goldfarb and Santosh, 2014; Zhang Z. et al., 2019; Liu et al., 2019, 2020; Li J. et al., 2020; Deng et al., 2020), and the Cu-Au-Fe polymetallic Middle-Lower Yangtze River Metallogenic Belt (MLYRB) (e.g., Pirajno and Zhou, 2015; Zhou et al., 2015; Zhang Y. et al., 2019; Lü et al., 2021). Many of these deposits are closely related in space-time to adakitic magmatism, yet many adakitic units in the region are also ore-barren (e.g., Liu S.-A. et al., 2010; Li C. et al., 2020; Jiang et al., 2020). Genetic link between adakitic magmatism and Cu-Au mineralization is rather well-established (e.g., Reich et al., 2003; Richards and Kerrich, 2007; Chiaradia et al., 2012), yet understanding why some adakites are ore-barren would also benefit both ore deposit modelling and regional Cu-Au exploration (**Table 1**).

In the southeastern NCC margin (Anhui province) where the North China Alluvial Plain is currently situated, intrusive rocks are rarely exposed and thus less studied. In this study, we collected samples from various underground coal mines across the Huaibei-Linhuan coalfield (**Figure 1**). Through zircon U-Pb dating and whole-rock geochemical analyses, and by comparing geochemically with the coeval Cu-Au mineralized/barren adakites across Eastern China (esp. in the MLYRB and along/near the southern Tanlu fault), we discuss why some adakites are ore-forming and some are not.

TABLE 1 | Summary of ages, intrusions and lithology of major barren and fertile adakite units in Eastern China.

No.	Location	Intrusion	Lithology	Ages (Ma)	Barren or fertile	Source
1	BWGB	Caoshan	Monzogranite	109 ± 3	Au	Li et al. (2020a)
2		Donglushan	Diorite porphyry	113 ± 1		
3		Jiangshan	Altered granite porphyry	117 ± 3		
4		Jiuhuashan	Granodiorite	115 ± 3		
5		Huaiguang	Granodiorite	118 ± 3		Liu et al. (2012)
6		Jingshan	Granodiorite	118 ± 1		
7		Zhuishan	Monzogranite	112 ± 1		
8		Caoshan	Monzogranite	112 ± 2		Yang et al. (2010)
9		Huaiguang	Granodiorite	130 ± 2		
10		Nvshan	Syenogranite	130 ± 3		
11	STLF	Damaocun	Monzonite	128 ± 1	Ore-Barren	Liu et al. (2010a)
12		Fangjiazhuang	Monzonite	129 ± 1		
13		Xiaolizhuang	Quartz monzonite	125 ± 1		
14		Qiaotouji	Monzonite	132 ± 2		
15		Haizi	Diorite	130 ± 2		In this study
16		Taiping	diorite	129 ± 1		
17		Qingdong	Microgabbro	116 ± 1		
18		Yuan-1	dolerite	106 ± 2		
19	MLYRB	Datuanshan	Carbonate	139 ± 3	Cu-Au-Mo	Mao et al. (2006)
20		Tongguanshan	Granodiorite	137 ± 1	Cu-Au	Jiang et al. (2020)
21		Longhushan	Diorite	138 ± 3	Cu-Au-Mo	Sun et al. (2003)
22		Shanxingshan	Granodiorite	138 ± 3	Mo	
23		Xianlinbu	Granodiorite	133 ± 1	Fe-Mo	
24		Yueshan	Quartz diorite	136 ± 2	Cu-Mo	
25		Fengshandong	Granodiorite	144 ± 2	Cu-Mo	Xie et al. (2007)
26		Qianjiawan	Diorite	138 ± 2	Cu-Au	
27		Ruanjiawan	Granodiorite	144 ± 2	W-Cu-Mo	
28		Tongshankou	Granodiorite	142 ± 2	Cu-Mo	
29		Tonglüshan	Granodiorite	138 ± 2	Cu-Fe	
30	DOB	Liujiawa	Gabbronorite	128 ± 1	Ore-Barren	Zhang et al. (2013)
31		Liujiawa	Diorite	127 ± 2		
32		Liguo	Dioritic porphyry	131 ± 3	Fe	Xu et al. (2004)
33		Jiagou	Monzodioritic porphyry	132 ± 4	Ore-Barren	
34		Banjing	Diorite	126 ± 2		Zhou et al. (2019)
35		Banjing	Diorite	127 ± 1		Yang et al. (2008)
36		Fengshan	Monzodiorite porphyry	129 ± 2		
37		Caishan	Quartz diorite	131 ± 1		

**BWGB: Bengbu-Wuhe Gold Belt; STLF: Southern Tan-Lu Fault; MLYRB: Middle-Lower Yangtze River Metallogenic Belt; DOB: Dabie Orogen Belt.*

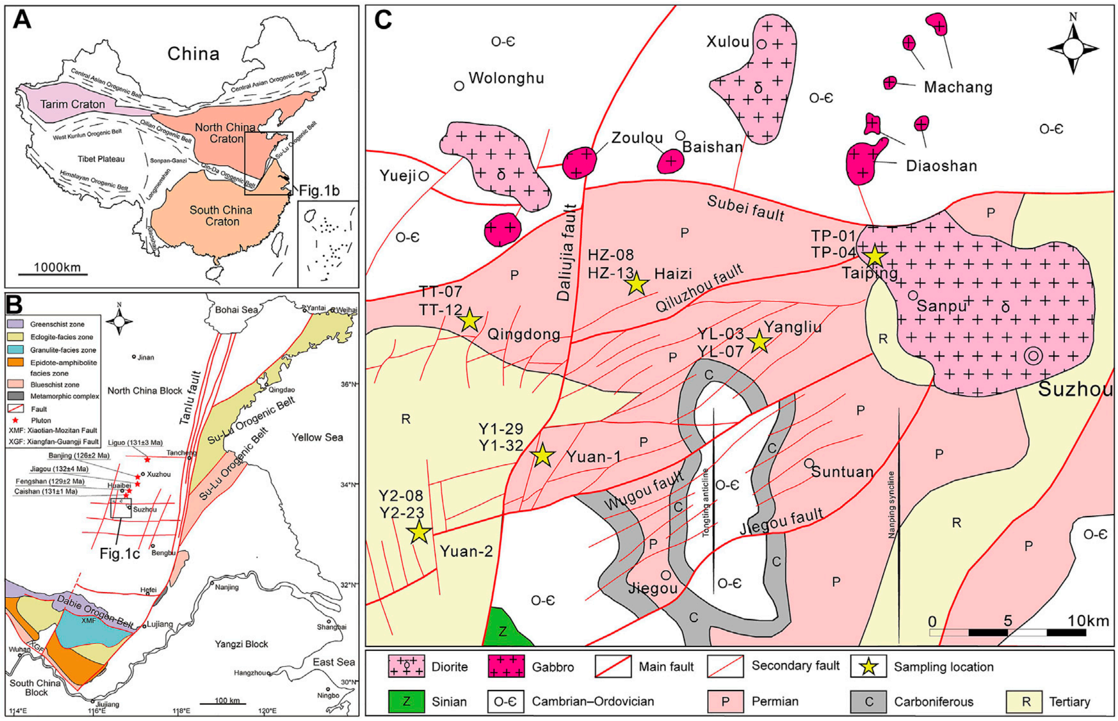

FIGURE 1 | Tectonic maps of China **(A)** and North China **(B)**, and **(C)** geologic map of the Huaibei-Linhuan coalfield, showing the distribution of basement rocks, sampling sites and major structures (modified after Zhao et al., 2016; Zhu et al., 2005, 2009; An et al., 2018).

Geological Background

Archean to Mesozoic geological record is well-preserved in the NCC, except locally in its eastern part due to later decratonization. The craton was largely formed by extensive Archean tonalite-trondhjemite-granodiorite (TTG) emplacement, and remained relatively stable throughout the Paleozoic-Early Triassic. Afterward, the convergence between the Yangtze and North China plates (collided in the Early-Middle Jurassic) had caused widespread Mesozoic magmatism, forming the Cretaceous intermediate-mafic and bimodal (sub-) volcanic rocks in the southern NCC margin (Li et al., 2017). Some intrusive rocks were suggested to have formed by mantle underplating and had a crustal-mantle mixed source. Geochemistry of these rocks implies that the lithospheric mantle beneath the NCC is highly heterogenous (Yang et al., 2008; Zhao et al., 2009; Xia et al., 2013).

Although igneous rock exposure is generally poor in the southeastern NCC margin, many intrusions are encountered in the underground coal mines there, notably those in the Huaibei-Linhuan coalfield. The Huaibei coalfield is located close to the Xuzhou–Suzhou fault system and between the EW-trending Fengpei and Bangpu uplift zones (**Figure 1B**). Faults of various sizes and types were documented in the coalfield, but consist mainly of high-angle normal faults and rare reverse faults. The regional Huangji and Subei faults were interpreted to have formed in the same stage as the regional Carboniferous-Permian folding (which formed the Tongting syncline and Nanping anticline) (**Figure 1C**) (An et al., 2018).

The Linhuan coalfield is bounded by the N-S-trending Taihe-Wuhe and Subei faults, and by the E-W-trending Nanping and Fengwo faults, giving a rectangular shape to the coalfield. The Taihe-Wuhe fault is a steeply-dipping normal fault, which connects to the Tanlu fault zone in the east. Secondary faults and interlayer structures are well-developed in the coalfield: the former is mainly NE-trending and less-commonly NW-trending, whilst the latter is developed on both hanging-wall and footwall of the coal seams, which locally damaged the coal seams. Major fault activities likely commenced in the Jurassic (early-stage Yanshanian orogeny), during which the regional stress transition (to NW-SE-trending) may have formed the Xuzhou-Suzhou imbricated structure. Tectonic regime in Eastern China changed again to active extension during the middle- and late-stage Yanshanian orogeny, forming many normal faults and fault-bounded basins. Normal faulting likely reached its peak during the Cenozoic Himalayan orogeny, during which many ancient structures were also reactivated/modified (Yao and Liu, 2012). Intermediate volcanism and plutonism were active during the Yanshanian movement, and were mainly controlled by the NNE-trending and EW-trending faults (Xu et al., 2004; Yang et al., 2010).

Previous geological survey documented that stratigraphy in the Linhuan coalfield comprises Ordovician and Carboniferous-Permian sequences (#3 Exploration Team of Anhui Bureau of Coal Geology, 2007). The coal-bearing sequences include the Upper Carboniferous Benxi and Taiyuan formations, Lower Permian Shanxi Formation, Middle Permian Shihezi

Formation, and the Middle-Upper Permian Shiqianfeng Formation. The Carboniferous sequences comprise mainly greyish mudstone in the lower part, and crystalline limestone and sandy shale-mudstone in the upper part. The Permian sequences comprise mainly sandstone and mudstone (An et al., 2018, and ref. therein). Plutonic emplacement is locally controlled by ancient faults and interlayer fractures, which likely served as magma conduits. Many Jurassic-Cretaceous intermediate-mafic dykes were identified in the Huaibei coalfield, and are controlled mainly by NNE-trending faults and minor by EW-trending and NW-trending ones. Middle Jurassic-Early Cretaceous intermediate-felsic plutons are widespread in the southern NCC margin, and eclogite xenoliths and adakitic rocks were reported in the Xuhuai area as a rectangle tectonic region in the Southern Tan-Lu Fault (STLF) showing in **Figure 1B** (Xu et al., 2006; Xu et al., 2009). Plutonic rocks intruding the coal-bearing sequence in the Huaibei coalfield include mainly diorite porphyry stock, dykes, and sills. All coal mines in the Linhuan coalfield were affected (metamorphosed) by various degrees of plutonism, which intensified toward the Subei and Daliujia faults, e.g., at the Yangliu and Haizi mines (#3 Exploration Team of Anhui Bureau of Coal Geology, 2007; Yangliu Coal Industry Co. Ltd, 2017; Zhao et al., 2019).

Intrusive rock samples in this study were collected from coal mines in the Huaibei-Linhuan coalfield. Plutons are mainly dioritic in the coal mines along the NE-trending Qiluzhou fault (Taiping, Haizi, Yangliu), whilst those in the coal mines along the NS-trending Daliujia fault (Yuandian-1, Yuandian-2, Qingdong) are mainly gabbroic and minor peridotitic.

Sampling and Analysis Methods

In this study, we analyzed igneous rock samples from six mines in the Huaibei-Linhuan coalfield, with the sampling locations shown in **Figure 1C**. Sample lithologies include (quartz-) diorite-granodiorite (n = 6) from Yangliu (YL-03, YL-07), Haizi (HZ-08, HZ-13), and Taiping (TP-01, TP-04), and microgabbro-dolerite (n = 6) from Qingdong (TT-07, TT-12), Yuandian-1 (Y1-29, Y1-32), Yuandian-2 (Y2-08, Y2-23). The rock samples were prepared into petrographic thin sections and rock powder (200 mesh) for microscopic (including SEM) observations and whole-rock geochemical analyses, respectively. Sample preparation and petrographic observation were conducted at the Geological Laboratory of the School of Resources and Environment Engineering, Anhui University. Optical microscopic analysis was performed with an Olympus BX53PLM to identify textural features and rock-forming minerals. Whole-rock major and trace elemental compositions were measured on all samples by X-ray fluorescence (XRF) and inductively coupled plasma mass spectrometry (ICP-MS), respectively.

The XRF analysis follows the Chinese national standard procedure GB/T 14506.28-2010. The powdered samples were dried at 105°C for 2–4 h and then cooled down in a desiccator. For each sample, 0.700 g was weighted and mixed with 5.200 g $Li_2B_4O_7$, 0.400 g LiF, and 0.300 g NH_4NO_3. The mixture was placed in platinum crucibles (95% Pt + 5% Au). Afterward, 1 ml LiBr (1.5%) was added to the crucibles, dried on a hot-plate, and then heat (with lid closed) at 1,200°C for 10 min to form a glass disc.

Solution ICP-MS sample preparation follows the Chinese National Standard Procedure GB/T 30714-2014. Weighted dry sample powder (0.1000 g) was placed in polytetrafluoroethylene (PTFE) bottles, mixed successively with 10 ml HNO_3, 10 ml HF, and 2 ml HCl, and then heated on hot-plate for 2–3 h to completely dissolve the samples. After cooling, the residue was washed with ultra-pure water, dried again, and then redissolved in 2.0 ml aqua reqia and 1.0 ml LH_3BO_3 on hot-plate for around 16 min. The solution was then transferred to 50 ml bottles, diluted with water and then measured (with two blanks) on an Agilent 7700e ICP-MS. The analysis follows the Chinese national standard procedure DZ/T0223-2001.

LA-ICP-MS zircon U-Pb dating was performed at the Wuhan Sample Solution Analytical Technology Co. Ltd. (China) with an Agilent 7900 ICPMS, coupled to a GeoLas HD 193 nm excimer laser ablation system. Zircon 91500 and glass NIST610 were used as external standards for U-Pb dating and trace element calibration, respectively. Each analysis incorporated a background acquisition of approximately 20–30 s followed by 50 s of data acquisition from the sample. An Excel-based software ICPMSDataCal was used to perform off-line selection and integration of background and analyzed signals, time-drift correction and quantitative calibration for trace element analysis and U-Pb dating (Liu et al., 2008; Liu et al., 2010 Y.). Concordia diagrams and weighted mean calculations were made using Isoplot/Ex_ver3 (Ludwig, 2003). Analytical conditions include: 80 mJ laser energy, 5 Hz frequency, and 32 μm laser beam size. The standards were analyzed twice for every six samples. The data processing and concordia plot production were completed with ICPMSDataCal 10.9 and Isoplot 3.0, respectively.

RESULTS

Petrographic Features

Taiping mine: Diorite samples were collected from a dyke (4–6 m thick) at 300 m depth. The rocks are dark-grey, medium-fine-grained, and massive structure. The rocks contain mainly plagioclase (75%) and hornblende (20%) and rare pyroxene (<5%). Some samples are porphyritic and have zoned plagioclase phenocrysts in a dark grey to greyish-green microcrystalline groundmass. The plagioclase grains are largely euhedral-subhedral, whilst hornblende grains are subhedral (**Figures 2A,D**).

Yangliu mine: The diorite-granodiorite samples were collected from a sill at 463–504 m depth (drill-hole 2017-02). The rocks are weakly porphyritic, with subrounded quartz and alkali feldspar phenocrysts and (minor) hornblende phenocrysts set in a dark-grey hornblende groundmass. Feldspar phenocrysts (2 mm) are generally larger than subhedral hornblende phenocrysts (0.5 mm) (**Figures 2C,F**).

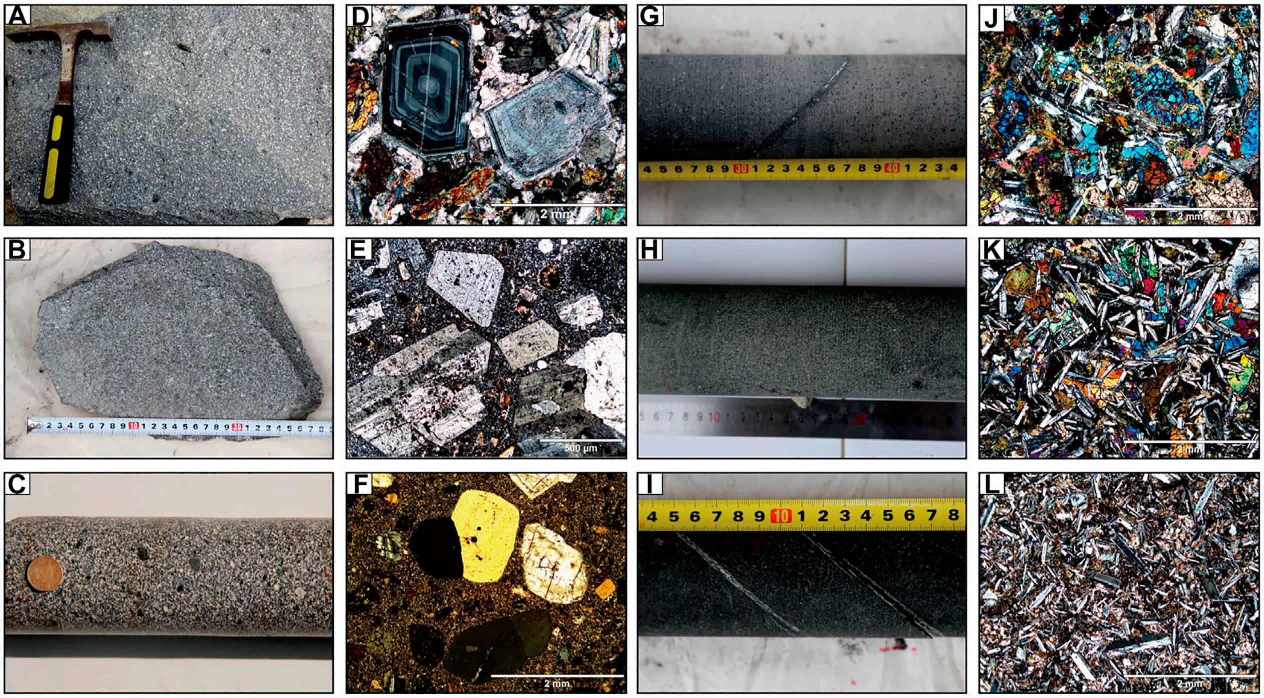

FIGURE 2 | Hand-specimen and thin-section microscopic photos of subvolcanic rocks from the Huaibei-Linhuan coalfield: **(A)** Taiping (TP-01) diorite; **(B)** Haizi (HZ-08) diorite; **(C)** Yangliu (YL-03) diorite; **(D)** Taiping granodiorite with feldspar phenocrysts; **(E)** Haizi porphyritic diorite with altered euhedral feldspar phenocrysts; **(F)** Yangliu granodiorite porphyry with quartz and plagioclase phenocrysts; **(G)** Qingdong (TT-07) microgabbro; **(H)** Yuandian-1 (Y1-29) dolerite; **(I)** Yuandian-2 (Y2-23) dolerite; **(J)** Pyroxene and plagioclase in the Qingdong microgabbro (XPL); **(K)** Plagioclase and pyroxene in the ophitic-textured Yuandian-1 dolerite (XPL); **(L)** Plagioclase and fine-grained Fe-Ti oxides in the Yuandian-2 dolerite (XPL).

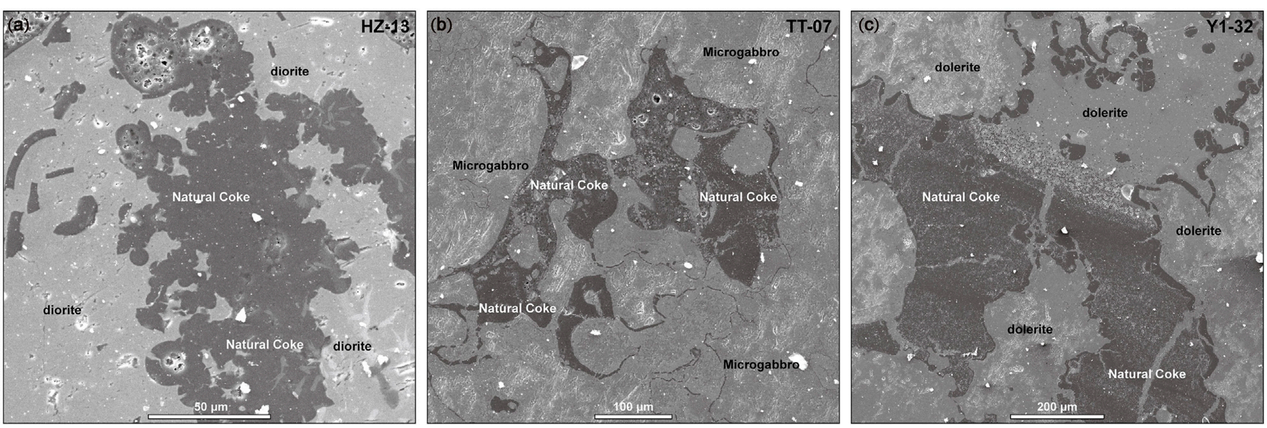

FIGURE 3 | SEM image of plutonic rock samples, showing partially-assimilated porous natural coke inclusions with rounded corroded margin: **(A)** HZ-13; **(B)** TT-07; **(C)** Y1-32.

Haizi mine: The diorite porphyry samples were collected from a dyke (8–10 m thick) at 800 m depth. The rocks are dark grey and medium-fine-grained massive, and contain mainly phenocrysts of plagioclase (60%), hornblende (20%) and pyroxene (<5%), which set in a dark-grey hornblende and (minor) pyrite groundmass (**Figures 2B,E**). Partially assimilated porous and rounded-/irregular-shaped natural coke fragments are included in the diorite (**Figure 3A**).

Qingdong mine: The microgabbro samples were collected from a sill at 478–483 m depth (drill-hole 2016-03). The rocks are greyish-green, fine-grained massive, and contain mainly plagioclase feldspars (55%), pyroxene (35%) and olivine (10%) (**Figures 2G,J**). Partially assimilated natural coke fragments, featured by being porous and rounded/irregular, are observed under SEM in the microgabbro (**Figure 3B**).

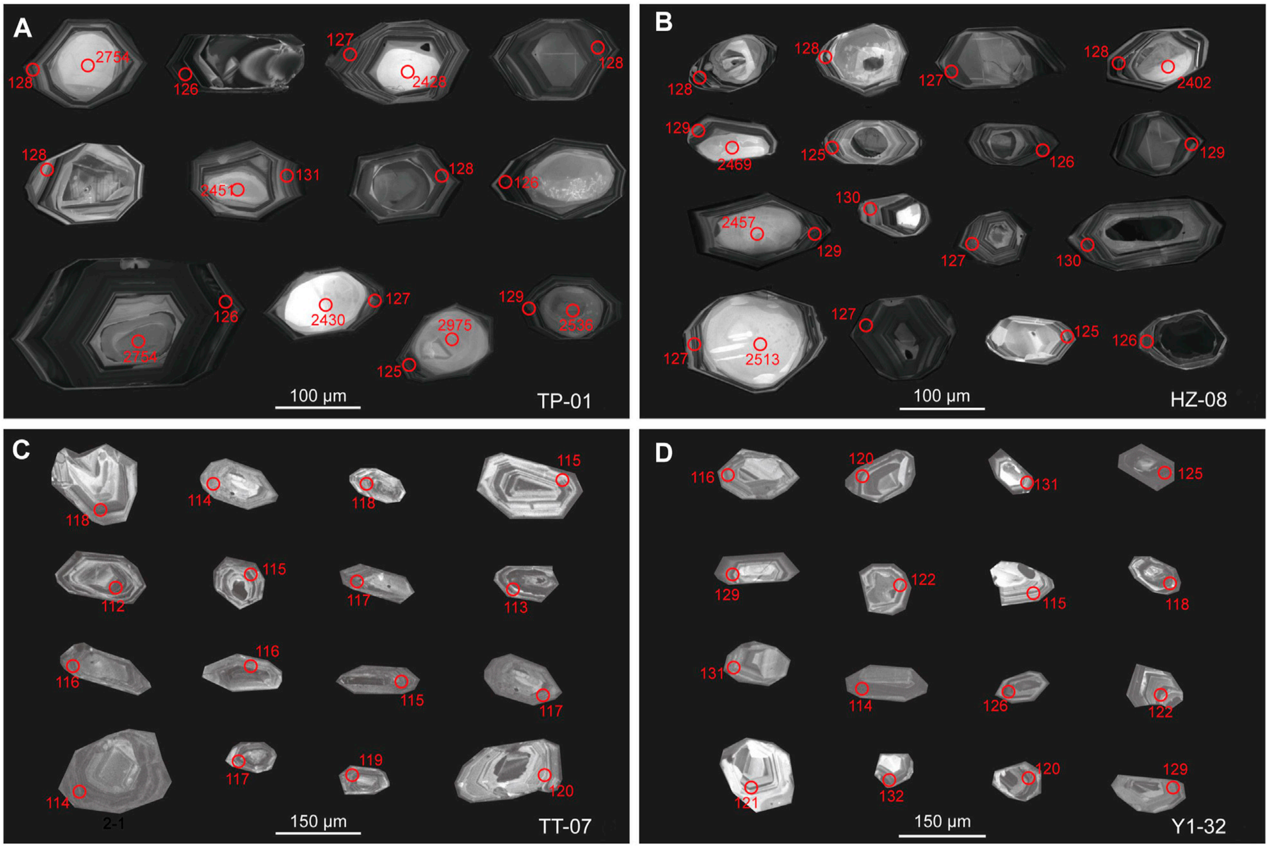

FIGURE 4 | Representative zircon CL images for the Huaibei-Linhuan intrusive rock samples: **(A)** Taiping diorite (TP-01); **(B)** Haizi diorite porphyry (HZ-08); **(C)** Qingdong microgabbro (TT-07); **(D)** Yuandian-1 dolerite (Y1-32).

Yuandian-1 mine: The dolerite samples were collected from a sill at 295–320 m depth (drill-hole 2016-06). The rocks are greyish-green, fine-medium-grained massive (weakly porphyritic), and contain euhedral-subhedral plagioclase (65%) and pyroxene (25%) phenocrysts set in a groundmass (10%) of similar mineral content (**Figures 2H,K**). Some dolerite samples contain partially assimilated natural coke fragments (**Figure 3C**).

Yuandian-2 mine: The dolerite samples were collected from a sill at 278–305 m depth (drill-hole 2016-20). The rocks are greyish-green, fine-medium-grained massive, and weakly porphyritic. The rocks have mainly plagioclase (60%), pyroxene (20%), and minor (10% each) hornblende and Fe-Ti oxides. The pyroxenes are commonly altered to fine-grained amphibole and chlorite (**Figures 2I,L**).

Zircon U-Pb Geochronology and Trace Element Geochemistry

In this study, one Taiping diorite (TP-01) and Haizi diorite porphyry (HZ-08), and one Qingdong microgabbro (TT-07) and Yuandian-1 dolerite (Y1-32) were zircon U-Pb dated. Zircon grains from all rock samples are largely similar in size (50–150 μm, mostly ~100 μm). Zircons from the diorite samples (TP-01 and HZ-08) are featured by rounded, partially resorbed inherited cores (20–120 μm, mostly 25–90 μm) surrounded by oscillatory zoned rims, giving an overall short prismatic or subrounded shape. Most zircon cores have markedly different CL reflectance (darker or brighter) from their growth rims. The cores are mostly unzoned (homogenous) but sector zoning is also found in certain grains. For the microgabbro-dolerite samples (TT-07 and Y1-32), most zircon grains do not have inherited core, and most of them are elongated prismatic (some occur as broken fragments), and are oscillatory- and/or sector-zoned (**Figure 4**).

Zircon samples from the Taiping diorite (TP-01) have high Th/U ratios for both the inherited cores (avg. 0.62) and rims (avg. 0.39), resembling typical igneous zircons (Hoskin and Black, 2000). Most age data (n = 19) from the cores cluster closely around 2,500 Ma, and yielded an upper intercept $^{206}Pb/^{238}U$ age of 2,463 ± 23 Ma (2σ, MSWD = 1.2). Meanwhile, age data (n = 21) from the rims yielded a weighted average $^{206}Pb/^{238}U$ age of 129.2 ± 1.4 Ma (2σ, MSWD = 2.0), which we interpreted to be the diorite emplacement age (**Figures 4A**, **5B**; **Table 2**).

Similarly, zircons from the Haizi diorite porphyry (HZ-08) have high Th/U ratios for both the inherited cores (avg. 0.47) and rims (avg. 0.84), resembling typical igneous zircons (Hoskin and Black, 2000). Age data (n = 19) from the cores also cluster closely around 2,500 Ma, and yielded an upper intercept $^{206}Pb/^{238}U$ age

TABLE 2 | Zircon U-Pb dating results of the plutonic rock samples from the Huaibei-Linhuan coalfield.

Spot No.	Hf	Ti	Th	U	Th/U	Isotopic ratios						Apparent ages (Ma)						Concordance
	ppm					207Pb/206Pb	1σ	207Pb/235U	1σ	206Pb/238U	1σ	207Pb/206Pb	1σ	207Pb/235U	1σ	206Pb/238U	1σ	
HZ-08C																		
HZ-08C-01	9202	11.7	38.1	31.9	1.19	0.1698	0.0056	9.8772	0.3195	0.4218	0.0063	2567	54.9	2423	29.9	2269	28.5	93%
HZ-08C-02	8414	14.0	19.5	38.8	0.50	0.1514	0.0048	9.0596	0.2811	0.4333	0.0067	2361	53.7	2344	28.4	2321	30.0	98%
HZ-08C-03	9685	17.7	1.10	16.2	0.07	0.1555	0.0070	9.3553	0.4266	0.4357	0.0095	2409	77.3	2373	41.9	2331	42.5	98%
HZ-08C-04	8435	9.86	17.4	33.1	0.53	0.1655	0.0063	10.0419	0.3869	0.4392	0.0068	2513	63.9	2439	35.6	2347	30.6	96%
HZ-08C-05	10905	7.35	55.1	76.1	0.72	0.1608	0.0043	9.8848	0.2764	0.4414	0.0058	2465	44.3	2424	25.8	2357	26.1	97%
HZ-08C-06	10007	11.6	2.03	12.0	0.17	0.1777	0.0083	10.7186	0.4708	0.4462	0.0094	2632	77.8	2499	40.8	2378	41.8	95%
HZ-08C-07	9240	14.5	15.1	66.3	0.23	0.1702	0.0047	10.6386	0.2957	0.4517	0.0057	2561	46.3	2492	25.9	2403	25.6	96%
HZ-08C-08	11063	13.4	202	221	0.91	0.1695	0.0048	10.7218	0.3114	0.4563	0.0049	2554	46.8	2499	27.0	2423	21.8	96%
HZ-08C-09	9515	10.6	6.70	6.71	1.00	0.1683	0.0105	10.5411	0.6338	0.4597	0.0114	2543	104.9	2484	55.8	2438	50.2	98%
HZ-08C-10	10489	13.0	9.04	22.0	0.41	0.1674	0.0067	10.4505	0.3924	0.4608	0.0078	2532	67.9	2476	34.8	2443	34.3	98%
HZ-08C-11	8966	68.1	13.5	29.2	0.46	0.1659	0.0129	10.0351	0.7138	0.4623	0.0124	2516	131.3	2438	65.7	2450	54.5	99%
HZ-08C-12	9849	10.8	40.7	28.1	1.45	0.1674	0.0058	10.7327	0.3832	0.4637	0.0068	2532	59.1	2500	33.2	2456	30.0	98%
HZ-08C-13	8861	15.2	16.0	26.5	0.61	0.1638	0.0064	10.5249	0.4005	0.4663	0.0078	2495	65.4	2482	35.3	2467	34.3	99%
HZ-08C-14	10590	15.4	4.95	35.6	0.14	0.1594	0.0052	10.3533	0.3701	0.4686	0.0081	2450	55.6	2467	33.1	2477	35.6	99%
HZ-08C-15	9520	18.4	0.70	4.15	0.17	0.1674	0.0113	10.6939	0.7166	0.4698	0.0158	2531	113.3	2497	62.2	2483	69.5	99%
HZ-08C-16	10230	14.3	6.83	37.7	0.18	0.1640	0.0083	10.3934	0.5197	0.4726	0.0124	2498	85.8	2470	46.3	2495	54.2	99%
HZ-08C-17	9967	16.1	10.1	13.0	0.78	0.1660	0.0080	10.6766	0.4762	0.4780	0.0094	2518	81.6	2495	41.4	2519	41.0	99%
HZ-08C-18	10287	24.9	0.99	8.71	0.11	0.1704	0.0101	10.9619	0.5897	0.4809	0.0116	2561	99.1	2520	50.1	2531	50.5	99%
HZ-08C-19	10707	23.2	102	61.5	1.66	0.1611	0.0043	10.9327	0.2949	0.4893	0.0066	2478	50.2	2517	25.2	2568	28.6	98%
HZ-08E																		
HZ-08E-01	9648	4.51	352	445	0.79	0.0501	0.0035	0.1335	0.0087	0.0202	0.0003	211	161.1	127	7.8	126	2.1	98%
HZ-08E-02	13442	2.96	122	515	0.24	0.0507	0.0034	0.1396	0.0082	0.0201	0.0004	233	157.4	133	7.3	128	2.7	96%
HZ-08E-03	7422	4.62	145	273	0.53	0.0501	0.0040	0.1368	0.0099	0.0199	0.0004	198	-13.9	130	8.9	127	2.4	97%
HZ-08E-04	9026	5.03	185	232	0.80	0.0465	0.0066	0.1365	0.0172	0.0209	0.0005	20.5	311.1	130	15.3	133	3.3	97%
HZ-08E-05	10358	0.93	84.0	245	0.34	0.0497	0.0045	0.1329	0.0113	0.0196	0.0004	189	200.0	127	10.1	125	2.4	98%
HZ-08E-06	9409	4.37	156	386	0.41	0.0514	0.0036	0.1378	0.0090	0.0197	0.0003	257	161.1	131	8.0	126	2.1	95%
HZ-08E-07	8070	4.46	131	154	0.85	0.0472	0.0039	0.1374	0.0102	0.0209	0.0004	61.2	194.4	131	9.1	133	2.7	98%
HZ-08E-08	9950	4.28	206	407	0.51	0.0486	0.0032	0.1296	0.0077	0.0197	0.0003	128	148.1	124	6.9	126	2.1	98%
HZ-08E-09	8842	6.16	232	312	0.75	0.0488	0.0035	0.1410	0.0086	0.0212	0.0004	200	98.1	134	7.6	135	2.2	99%
HZ-08E-10	9824	3.68	282	360	0.78	0.0490	0.0033	0.1345	0.0088	0.0199	0.0003	150	148.1	128	7.9	127	2.1	99%
HZ-08E-11	9396	7.97	164	334	0.49	0.0484	0.0035	0.1373	0.0088	0.0207	0.0004	120	159.2	131	7.9	132	2.2	99%
HZ-08E-12	9953	3.65	173	233	0.74	0.0482	0.0037	0.1334	0.0085	0.0203	0.0005	106	174.0	127	7.6	129	3.0	98%
HZ-08E-13	8972	7.31	84.7	270	0.31	0.0502	0.0043	0.1336	0.0102	0.0199	0.0003	206	185.2	127	9.1	127	2.1	99%
HZ-08E-14	12243	3.34	136	592	0.23	0.0482	0.0025	0.1307	0.0069	0.0199	0.0003	109	118.5	125	6.2	127	1.7	98%
HZ-08E-15	9478	3.49	120	270	0.44	0.0508	0.0041	0.1411	0.0105	0.0204	0.0003	232	187.0	134	9.3	130	2.2	96%
TP-01C																		
TP-01C-01	9812	11.2	54.4	148	0.37	0.1622	0.0040	9.6579	0.2312	0.4273	0.0042	2480	41.7	2403	22.1	2293	19.0	95%
TP-01C-02	11862	46.1	78.0	112	0.70	0.1601	0.0043	9.7043	0.2768	0.4334	0.0061	2457	45.4	2407	26.3	2321	27.6	96%
TP-01C-03	10709	14.7	63.0	43.2	1.46	0.1526	0.0053	9.3034	0.3231	0.4378	0.0062	2376	59.3	2368	31.9	2341	27.8	98%
TP-01C-04	10216	19.2	6.42	12.9	0.50	0.1613	0.0096	9.6874	0.5697	0.4413	0.0116	2469	101.7	2406	54.1	2356	51.7	97%
TP-01C-05	10777	23.0	43.9	59.8	0.74	0.1646	0.0048	10.1085	0.2995	0.4430	0.0054	2506	48.5	2445	27.4	2364	24.3	96%
TP-01C-06	9021	15.0	42.2	50.8	0.83	0.1710	0.0055	10.6793	0.3476	0.4511	0.0055	2569	54.0	2496	30.3	2400	24.5	96%
TP-01C-07	10654	20.9	195	240	0.81	0.1588	0.0041	10.0017	0.2606	0.4526	0.0048	2444	44.0	2435	24.1	2407	21.2	98%
TP-01C-08	10236	12.6	85.7	139	0.61	0.1587	0.0036	10.1313	0.2214	0.4584	0.0043	2442	38.3	2447	20.3	2432	19.2	99%
TP-01C-09	9886	10.1	31.4	30.3	1.04	0.1603	0.0051	10.1053	0.3314	0.4599	0.0087	2461	53.2	2444	30.3	2439	38.6	99%
TP-01C-10	8881	8.33	17.1	26.0	0.66	0.1583	0.0068	9.9209	0.3932	0.4617	0.0081	2439	72.1	2427	36.6	2447	35.7	99%
TP-01C-11	9783	16.7	4.39	18.3	0.24	0.1610	0.0064	10.2574	0.4026	0.4635	0.0083	2466	67.0	2458	36.4	2455	36.6	99%
TP-01C-12	11068	16.8	3.65	13.2	0.28	0.1710	0.0087	10.7429	0.5027	0.4645	0.0097	2568	85.2	2501	43.5	2460	42.9	98%
TP-01C-13	9892	10.4	10.4	31.3	0.33	0.1638	0.0057	10.5364	0.3610	0.4676	0.0077	2495	59.0	2483	31.8	2473	33.8	99%
TP-01C-14	9439	12.0	12.7	19.5	0.65	0.1686	0.0070	10.8547	0.4109	0.4697	0.0077	2544	70.2	2511	35.2	2482	34.0	98%
TP-01C-15	10747	13.8	8.16	17.7	0.46	0.1578	0.0084	9.9969	0.5075	0.4702	0.0087	2432	90.7	2434	46.9	2484	38.2	97%
TP-01C-16	10470	6.92	66.4	40.6	1.63	0.1590	0.0049	10.4772	0.3237	0.4767	0.0082	2456	51.5	2478	28.7	2513	35.8	98%
TP-01C-17	10603	16.3	13.5	20.3	0.66	0.1586	0.0060	10.4191	0.3873	0.4788	0.0088	2443	63.9	2473	34.5	2522	38.2	98%
TP-01C-18	12589	22.5	33.7	50.0	0.67	0.1747	0.0046	11.5898	0.3030	0.4818	0.0061	2603	43.8	2572	24.5	2535	26.5	98%
TP-01C-19	11539	26.4	15.2	35.6	0.43	0.1557	0.0048	10.5203	0.3088	0.4906	0.0070	2410	46.8	2482	27.3	2573	30.3	96%

(Continued on following page)

TABLE 2 | (*Continued*) Zircon U-Pb dating results of the plutonic rock samples from the Huaibei-Linhuan coalfield.

Spot No.	Hf	Ti	Th	U	Th/U	Isotopic ratios						Apparent ages (Ma)						Concordance
	ppm					207Pb/206Pb	1σ	207Pb/235U	1σ	206Pb/238U	1σ	207Pb/206Pb	1σ	207Pb/235U	1σ	206Pb/238U	1σ	
TP-01E																		
TP-01E-01	9517	3.73	82.0	519	0.16	0.0503	0.0032	0.1401	0.0085	0.0204	0.0003	209	146.3	133	7.6	130	1.8	97%
TP-01E-02	11982	0.09	6.14	500	0.01	0.0489	0.0032	0.1374	0.0084	0.0205	0.0003	143	144.4	131	7.5	131	1.9	99%
TP-01E-03	9056	4.81	560	609	0.92	0.0507	0.0025	0.1436	0.0070	0.0204	0.0002	233	119.4	136	6.2	130	1.5	95%
TP-01E-04	10889	1.73	80.3	286	0.28	0.0504	0.0041	0.1428	0.0100	0.0212	0.0004	213	190.7	136	8.9	135	2.5	99%
TP-01E-05	8653	4.54	413	461	0.90	0.0489	0.0027	0.1350	0.0077	0.0200	0.0003	143	163.9	129	6.9	128	2.1	99%
TP-01E-06	9229	2.81	34.0	175	0.19	0.0478	0.0043	0.1382	0.0106	0.0213	0.0005	87.1	200.0	131	9.4	136	2.8	96%
TP-01E-07	8063	3.10	189	222	0.85	0.0532	0.0044	0.1422	0.0102	0.0197	0.0004	345	158.3	135	9.1	126	2.6	93%
TP-01E-08	9676	3.81	97.5	207	0.47	0.0508	0.0047	0.1379	0.0111	0.0201	0.0004	235	212.9	131	9.9	128	2.4	97%
TP-01E-09	9372	2.89	8.32	459	0.02	0.0477	0.0033	0.1272	0.0078	0.0198	0.0003	83.4	159.2	122	7.0	126	2.0	96%
TP-01E-10	9290	5.11	181	255	0.71	0.0501	0.0039	0.1340	0.0085	0.0199	0.0003	198	183.3	128	7.6	127	2.1	99%
TP-01E-11	9236	4.85	71.5	241	0.30	0.0500	0.0042	0.1347	0.0106	0.0200	0.0004	195	181.5	128	9.5	128	2.3	99%
TP-01E-12	10747	1.60	54.6	283	0.19	0.0484	0.0035	0.1315	0.0088	0.0201	0.0004	120	162.9	125	7.9	128	2.4	97%
TP-01E-13	9099	3.96	81.2	211	0.39	0.0523	0.0057	0.1383	0.0120	0.0203	0.0006	298	251.8	132	10.7	129	3.7	98%
TP-01E-14	9069	2.36	97.2	191	0.51	0.0503	0.0053	0.1359	0.0121	0.0205	0.0005	209	225.9	129	10.8	131	3.4	99%
TP-01E-15	10318	3.84	19.1	231	0.08	0.0483	0.0045	0.1340	0.0112	0.0200	0.0006	122	198.1	128	10.0	128	3.6	99%
TP-01E-16	10238	3.92	313	759	0.41	0.0479	0.0023	0.1318	0.0068	0.0198	0.0003	100	105.5	126	6.1	126	1.9	99%
TP-01E-17	10433	5.94	117	693	0.17	0.0480	0.0029	0.1307	0.0082	0.0197	0.0003	98.2	137.0	125	7.3	126	1.8	99%
TP-01E-18	12632	1.52	8.22	134	0.06	0.0507	0.0058	0.1344	0.0136	0.0200	0.0005	228	244.4	128	12.2	127	3.3	99%
TP-01E-19	10076	4.23	246	369	0.67	0.0491	0.0034	0.1291	0.0080	0.0195	0.0004	150	155.5	123	7.2	125	2.4	98%
TP-01E-20	11273	1.38	94.9	316	0.30	0.0502	0.0039	0.1343	0.0097	0.0196	0.0004	206	179.6	128	8.7	125	2.2	97%
TP-01E-21	10201	3.43	252	398	0.63	0.0535	0.0037	0.1462	0.0091	0.0202	0.0004	350	157.4	139	8.1	129	2.3	92%
TT-07																		
TT-07-01	9463	31.9	172	468	0.37	0.0502	0.0061	0.1188	0.0130	0.0175	0.0004	211	250.0	114	11.8	112	2.8	98%
TT-07-02	8566	10.3	220	471	0.47	0.0513	0.0037	0.1262	0.0077	0.0182	0.0003	254	168.5	121	7.0	116	2.1	96%
TT-07-03	9900	4.04	165	522	0.32	0.0536	0.0039	0.1380	0.0091	0.0188	0.0003	354	160.2	131	8.1	120	1.7	91%
TT-07-04	10312	4.36	299	647	0.46	0.0509	0.0026	0.1271	0.0059	0.0182	0.0003	235	112.0	122	5.3	116	1.7	95%
TT-07-05	9656	8.97	291	751	0.39	0.0525	0.0030	0.1316	0.0064	0.0184	0.0004	309	131.5	126	5.7	118	2.4	93%
TT-07-06	9716	2.83	157	535	0.29	0.0506	0.0037	0.1277	0.0083	0.0183	0.0004	233	163.9	122	7.5	117	2.3	95%
TT-07-07	9987	5.55	598	919	0.65	0.0491	0.0028	0.1198	0.0061	0.0177	0.0002	150.1	135.2	115	5.6	113	1.6	98%
TT-07-08	10001	4.85	385	809	0.48	0.0510	0.0043	0.1226	0.0084	0.0179	0.0004	243	196.3	117	7.6	114	2.4	97%
TT-07-09	9697	22.6	136	497	0.27	0.0479	0.0039	0.1187	0.0074	0.0184	0.0003	100	175.9	114	6.7	117	1.9	97%
TT-07-10	10525	4.85	163	567	0.29	0.0502	0.0034	0.1282	0.0076	0.0187	0.0002	206	163.9	123	6.9	119	1.6	97%
TT-07-11	10112	3.49	257	552	0.47	0.0516	0.0027	0.1268	0.0064	0.0179	0.0002	333	123.1	121	5.8	114	1.5	94%
TT-07-12	10407	4.75	303	761	0.40	0.0513	0.0026	0.1311	0.0062	0.0186	0.0002	254	118.5	125	5.6	119	1.6	94%
TT-07-13	9996	10.2	97.2	320	0.30	0.0507	0.0039	0.1258	0.0085	0.0181	0.0003	228	179.6	120	7.7	116	2.1	96%
TT-07-14	10493	671	171	564	0.30	0.0489	0.0057	0.1260	0.0147	0.0185	0.0002	143	251.8	120	13.2	118	1.5	97%
TT-07-15	10030	11.9	257	644	0.40	0.0516	0.0029	0.1267	0.0056	0.0178	0.0002	265	129.6	121	5.0	114	1.5	93%
TT-07-16	9353	2.97	282	258	1.09	0.0499	0.0035	0.1203	0.0076	0.0177	0.0004	187	166.6	115	6.9	113	2.6	97%
TT-07-17	10200	5.49	335	735	0.46	0.0471	0.0026	0.1155	0.0058	0.0178	0.0002	53.8	135.2	111	5.3	114	1.5	97%
TT-07-18	10096	9.84	244	695	0.35	0.0494	0.0033	0.1206	0.0070	0.0176	0.0003	165	157.4	116	6.3	113	1.8	97%
TT-07-19	10278	7.14	431	945	0.46	0.0511	0.0027	0.1289	0.0064	0.0183	0.0002	243	120.4	123	5.7	117	1.5	94%
TT-07-20	9952	5.49	190	484	0.39	0.0504	0.0036	0.1266	0.0082	0.0185	0.0003	213	166.6	121	7.4	118	1.7	97%
TT-07-21	9890	7.05	348	631	0.55	0.0498	0.0048	0.1167	0.0093	0.0173	0.0003	183	214.8	112	8.4	110	2.1	98%
TT-07-22	8864	7.73	434	234	1.86	0.0548	0.0047	0.1344	0.0090	0.0182	0.0004	406	194.4	128	8.0	116	2.7	90%
TT-07-23	10407	3.57	190	577	0.33	0.0503	0.0035	0.1212	0.0074	0.0175	0.0003	206	162.9	116	6.7	112	1.9	96%
TT-07-24	10213	7.26	313	794	0.39	0.0482	0.0026	0.1226	0.0058	0.0184	0.0003	109	122.2	117	5.2	117	1.7	99%
TT-07-25	9131	3.00	123	161	0.77	0.0518	0.0053	0.1274	0.0102	0.0183	0.0004	276	230.5	122	9.2	117	2.8	96%
Y1-32																		
Y1-32-01	9119	6.99	422	409	1.03	0.1471	0.0204	0.3196	0.0332	0.0180	0.0006	2313	239.7	282	25.6	115	3.8	16%
Y1-32-02	9518	9.99	703	581	1.21	0.0481	0.0028	0.1134	0.0059	0.0171	0.0002	106	129.6	109	5.4	109	1.4	99%
Y1-32-03	10079	66.0	375	395	0.95	0.1343	0.0090	0.3408	0.0218	0.0184	0.0003	2155	149.1	298	16.5	117	2.1	12%
Y1-32-04	7902	9.78	210	203	1.03	0.1273	0.0145	0.3210	0.0421	0.0177	0.0005	2061	197.2	283	32.4	113	3.4	14%
Y1-32-05	8864	55.5	273	311	0.88	0.0530	0.0066	0.1168	0.0116	0.0169	0.0004	328	287.0	112	10.6	108	2.6	96%
Y1-32-06	9254	2.26	219	347	0.63	0.0740	0.0146	0.1410	0.0168	0.0163	0.0005	1043	406.0	134	15.0	104	3.2	75%
Y1-32-07	9031	9.98	2493	1702	1.47	0.0765	0.0031	0.1770	0.0070	0.0167	0.0002	1107	76.9	166	6.1	107	1.3	57%
Y1-32-08	10201	7.23	408	544	0.75	0.1012	0.0051	0.2430	0.0114	0.0175	0.0003	1656	92.7	221	9.3	112	1.7	34%

(Continued on following page)

TABLE 2 | (*Continued*) Zircon U-Pb dating results of the plutonic rock samples from the Huaibei-Linhuan coalfield.

Spot No.	Hf	Ti	Th	U	Th/U	Isotopic ratios						Apparent ages (Ma)						Concordance
	ppm					207Pb/206Pb	1σ	207Pb/235U	1σ	206Pb/238U	1σ	207Pb/206Pb	1σ	207Pb/235U	1σ	206Pb/238U	1σ	
Y1-32-09	9542	8.31	201	252	0.79	0.1270	0.0099	0.3267	0.0285	0.0184	0.0004	2057	133.2	287	21.8	117	2.8	16%
Y1-32-10	10928	9.19	909	822	1.11	0.0534	0.0024	0.1209	0.0054	0.0164	0.0002	343	101.8	116	4.9	105	1.3	90%
Y1-32-11	11717	5.67	158	153	1.03	0.1229	0.0119	0.3277	0.0344	0.0188	0.0005	1999	172.4	288	26.3	120	3.3	17%
Y1-32-12	10030	5.01	378	564	0.67	0.0911	0.0064	0.2232	0.0156	0.0178	0.0003	1450	134.1	205	12.9	114	1.8	42%
Y1-32-13	9723	11.6	637	803	0.79	0.1959	0.0108	0.5297	0.0306	0.0195	0.0003	2792	90.4	432	20.3	124	1.9	−11%
Y1-32-14	10295	3.84	391	534	0.73	0.0496	0.0030	0.1178	0.0064	0.0175	0.0002	176	147.2	113	5.8	112	1.6	98%
Y1-32-15	9454	11.1	154	175	0.88	0.0615	0.0061	0.1414	0.0119	0.0175	0.0004	655	212.0	134	10.6	112	2.5	81%

of 2,475 ± 33 Ma (2σ, MSWD = 2.3). Analyses of the zircon rims (n = 15) yielded a weighted average $^{206}Pb/^{238}U$ age of 130.0 ± 2.4 Ma (2σ, MSWD = 2.4), which we interpreted to be the diorite crystallization age (**Figures 4B**, **5A**,C; **Table 2**).

For the Qingdong microgabbro (TT-07), the zircon ages range narrowly from 110.48 to 120.38 Ma and there are no old inherited zircons. The zircons are likely igneous due to their high Th/U ratios (avg. 0.50) and the ubiquitous igneous oscillatory zoning. Twenty-five analyses yielded a weighted average $^{206}Pb/^{238}U$ age of 115.8 ± 1.1 Ma (2σ, MSWD = 2.0), which likely reflects the timing of the microgabbro formation (**Figures 4C**, **5B**,**E**; **Table 2**).

For the Yuandian-1 dolerite (Y1-32), most zircon ages range narrowly from 104.38 to 124.48 Ma. Again, the zircons are likely igneous due to their high Th/U ratios (avg. 0.93) and their igneous oscillatory zoning. Fifteen analyses yielded a weighted average $^{206}Pb/^{238}U$ age of 105.8 ± 1.8 Ma (2σ, MSWD = 2.8), which is largely the same (within error) as the upper intercept $^{206}Pb/^{238}U$ age (106.6 ± 2.4 Ma) and likely represents the dolerite formation age (**Figures 4D**, **5F**; **Table 2**).

Most zircons, regardless of their host-rock types and ages, have similar left-inclining REE patterns and positive Ce anomalies (Ce^{4+}/Ce^{3+} = mostly 0.21–90.78), resembling typical igneous zircons (Belousova et al., 2002). LREE contents are mostly low (often below the detection limit), and the few zircons with abnormally high La content are likely caused by apatite inclusions (Lu et al., 2016). Different rock samples, however, have different zircon Eu anomalies: Zircon rims of samples HZ-08 and TP-01 have no discernible anomalies [δEu: (Eu*/Eu) = 0.42–0.86], whereas their Neoarchean-Paleoproterozoic cores have distinct negative anomalies (δEu = 0.03–0.48). Varying negative Eu anomalies are present for both samples TT-07 (δEu = 0.03–0.84) and Y1-32 (δEu = 0.12–0.55) (**Figure 6**; **Table 3**).

Whole-Rock Elemental Compositions

For the 12 samples analyzed, their whole-rock major element contents were back-calculated to 100 wt% to remove the volatile influence. A few samples yielded very high LOI (e.g., TT07 = 12.36 wt%, Y2-23 = 10.19 wt%), which we considered to be caused by the natural coke inclusions (instead of alteration/weathering), as demonstrated by the fresh igneous texture and partially-assimilated natural coke fragments observed under the SEM (**Figure 3**). The microgabbro-dolerite samples have SiO_2 = 42.58–50.88 wt%, Al_2O_3 = 12.22–14.55 wt%, MgO = 5.44–8.63 wt%, FeO_T = 6.99–14.68 wt%, and (Na_2O + K_2O) = 2.62–4.08 wt%, whilst the diorite-granodiorite (Haizi, Taiping, and Yangliu) samples have SiO_2 = 57.45–61.27 wt%, Al_2O_3 = 14.53–16.12 wt%, MgO = 2.87–4.63 wt%, FeO_T = 4.0–6.71 wt%, and (Na_2O + K_2O) = 6.45–9.15 wt% (**Table 4**).

In the Total Alkali-Silica (TAS) diagram, the gabbro-dolerite samples fall inside the (olivine-)gabbro fields (some marginally alkali), whilst the diorite-granodiorite samples fall inside the (quartz-)monzonite and syenite fields (**Figure 7A**). Similar results are shown in the immobile Zr/Ti vs. Nb/Y diagram, suggesting that alteration/weathering has no major influence on the major element geochemistry (**Figure 7B**). Both the gabbro-dolerite (ASI = 0.94–1.38) and diorite-granodiorite

(ASI = 1.09–1.42) are peraluminous (**Figure 7C**), with the former being calc-alkaline and latter high-K calc-alkaline (**Figure 7D**). The diorite-granodiorite samples have high Sr (>677.7 ppm) and low Y (<15.48 ppm) (Sr/Y = 49.97–106.95), showing adakitic affinity. In contrast, the gabbro-dolerite samples have lower Sr (<384.2 ppm) and higher Y (>24.13 ppm)(Sr/Y = 15.26–83.19, avg. 47), resembling normal arc magmatic rocks (**Figure 8A**). The gabbro-dolerite and diorite-granodiorite samples have similar total (Σ) REE contents [73.14–193.10 ppm (avg. 112.88) and 50.51–113.45 ppm (avg. 84.99), respectively] and chondrite-normalized REE patterns, which are featured by enrichments in LREE/MREE [$(La/Yb)_N$ = 4.27–17.85 and 8.63–10.62, respectively] and MREE/HREE [$(Dy/Yb)_N$ = 1.76–2.16 and 1.81–1.98, respectively] (**Tables 4**; **Figures 7–8**). In primitive mantle-normalized diagrams, both the gabbro-dolerite and diorite-granodiorite show large ion lithophile element (LILE) over high field strength element (HFSE) enrichments, as well as negative Ta-Nb and Ti anomalies and distinct positive Pb and Sr anomalies.

DISCUSSION

Multiphase Magmatism in the Huaibei-Linhuan Coalfield

Intrusive rocks dated in this study yielded at least two magmatic phases: The Early Cretaceous diorite-granodiorite ages (Haizi: 130.0 ± 2.0 Ma; Taiping: 129.2 ± 1.4 Ma), whilst the microgabbro-dolerite yielded Late Cretaceous ages (Qingdong: 115.8 ± 1.1 Ma; Yuandian-1: 105.8 ± 1.8 Ma). The Early Cretaceous Huaibei-Linhuan diorite-granodiorite are coeval with the high-Mg adakite-like diorite-granodiorite in the Liujiawa pluton (~128 Ma), which is located further southwest in the eastern Dabie Orogen close to the Tanlu fault zone (**Figure 1**) (Jiang et al., 2020). Also along the Tanlu fault, the ore-related Nvshan syenogranite and the Huaiguang granodiorite in the Bengbu-Wuhe goldfield (Anhui Province) were both dated to be ~130 Ma (Li C. et al., 2020). The Huaibei-Linhuan (quartz-)diorite-granodiorite are also of similar age (slightly younger) than the Tongguanshan Cu-Au ore-forming adakites (~136.7 Ma; Tongling orefield), and the ore-barren high-Mg adakitic plutons at Fangjiangzhuang (~129.1 Ma) and Qiaotouji (~131.7 Ma) in the MLYRB (Liu S.-A. et al., 2010; Jiang et al., 2020). This suggests that the emplacement of the Huaibei-Linhuan (quartz-)diorite and granodiorite was part of the extensive Early Cretaceous (high-Mg-)adakitic magmatism, which extended from the along the eastern MLYRB northward along the Tanlu fault. From Eastern China, the Tanlu fault zone likely continues NE-ward across the Bohai sea basin into NE China, although its northeastern-most end is yet to be well identified (Ye et al., 2021). Early Cretaceous adakitic granitoids were documented at Xiuyan (ca. 129–126 Ma) in the Liaodong Peninsula (NE China) (Dong et al., 2020), and Krinichnoye (131.4 Ma) in the southern Sikhote-Alin (SE Russia Far East). As to be discussed in the later section, we attributed this major regional adakitic magmatism as a product of Paleo-Pacific subduction and rollback and/or tearing, facilitated by the reactivation of the Tanlu fault zone movement.

The younger late-Early Cretaceous magmatic phase in Huaibei-Linhuan (Qingdong: 115.8 Ma; Yuandian-1: 105.8 Ma) was also reported elsewhere along the Tanlu fault. For instance, normal-arc-type granite- and diorite porphyries and monzogranite from the Bengbu-Wuhe goldfield were dated at ca. 112–114 Ma, and the associated Bengbu mafic dykes yielded similar Ar-Ar age (plateau: 111.8 ± 0.6 Ma; isochron: 109.6 ± 1.5 Ma) (Liu et al., 2012; Li C. et al., 2020).

Petrogenesis of the Huaibei-Linhuan Magmatic Rocks

In this study, we have identified an earlier adakitic (quartz-)diorite-granodiorite phase and a younger gabbro-dolerite phase for the Early Cretaceous magmatism in Huaibei-Linhuan. For the adakitic (quartz-)diorite-granodiorite, they have relatively high Mg (MgO = 2.87–4.63; Mg# = 0.65–0.76) and low K_2O/Na_2O (0.35–0.54), resembling typical adakites derived from oceanic slab melting. Such features are distinct from the adakites derived from melting of the thickened lower crust, notably those from the Bengbu-Wuhe goldfield situated in the interior of the North China Craton (**Figure 8**) (Li C. et al., 2020). It is not to say that there is no crustal influence in the Huaibei-Linhuan adakitic rocks, as evidence from the presence of Precambrian inherited cores (2,317–2,632 Ma) in the Cretaceous zircons. The weighted average ages of the inherited cores for the (quartz-)diorite-granodiorite samples from Haizi (2,475 ± 33 Ma) and Taiping (2,463 ± 23 Ma) are similar to the relict magmatic zircons in (ca. 2,455 and 2,716 Ma) from the Cenozoic (~1 Ma) Nushan basalts in the southeastern North China Craton (Ping et al., 2019), suggesting clear NCC crustal input for the Huaibei-Linhuan adakite formation. The lack of the clear correlation between the adakitic signature (Sr/Y) and fractional crystallization (SiO_2) suggest that the adakites were not formed by high-pressure fractionation (garnet and/or amphibole) (**Figure 7D**). This conclusion is also supported by the lack of upward-concave MREE-HREE pattern in the chondrite-normalized REE plots (**Figure 9**), or the lack of correlation between MREE/HREE (Dy/Yb) and fractionation (SiO_2), which would be expect for amphibole-garnet fractionation-derived adakites or normal calc-alkaline rocks (such as the Huaibei-Linhuan gabbro-dolerite) (Castillo et al., 1999; Kamvong et al., 2014) (**Figure 10A**). Previous studies suggested that if the adakites were formed by fractional crystallization, substantial amphibole (85%) and garnet (15%) fractionation are needed (Mori et al., 2007). Our (quartz-)diorite-granodiorite samples do not fall on these fractionation trends (**Figures 10A–B**), and no garnet (and very few amphibole) was found in the rocks, suggesting that the adakites were not formed from fractional crystallization. In the Rb/Y vs. Nb/Y and Ba/Th vs. Th discrimination plots, the Huaibei-Linhuan adakite samples fall between the slab-derived and melt-derived enrichment trends, suggesting that the magmas were sourced from both slab-derived fluids and melts (**Figures 10C–D**). The Sr/La ratio has been used to distinguish slab-derived adakites

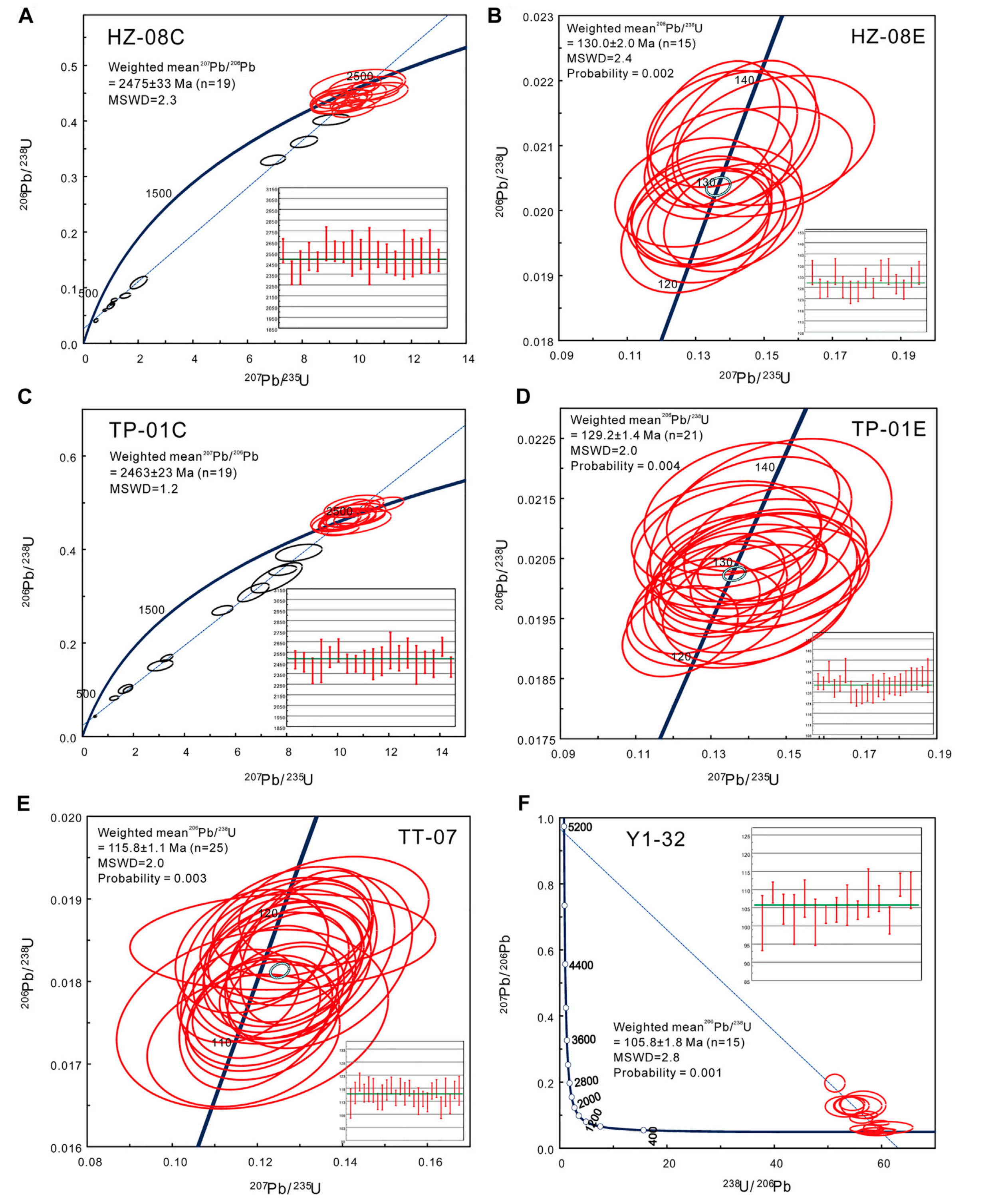

FIGURE 5 | Zircon LA-MC-ICP-MS U-Pb Concordia diagrams of the Huaibei-Linhuan intrusive rock samples: **(A)** inherited zircon cores from Haizi diorite porphyry (HZ-08); **(B)** zircon growth rims from Haizi diorite porphyry (HZ-08); **(C)** inherited zircon cores from Taiping diorite (TP-01); **(D)** zircon growth rims from Taiping diorite (TP-01); **(E)** Qingdong microgabbro (TT-07); **(F)** Yuandian-1 dolerite (Y1-32).

from lower-continental crustal (LCC)-derived ones, because altered oceanic crust (with MORB-type LREE depletion and Sr enrichment by seawater) has much higher Sr/La than the LCC (Liu S.-A. et al., 2010). Our adakitic (quartz-)diorite-granodiorite samples have elevated Sr/La ratios (**Figure 11A**), indicating a slab-derived origin. The slab-derived origin is also supported by

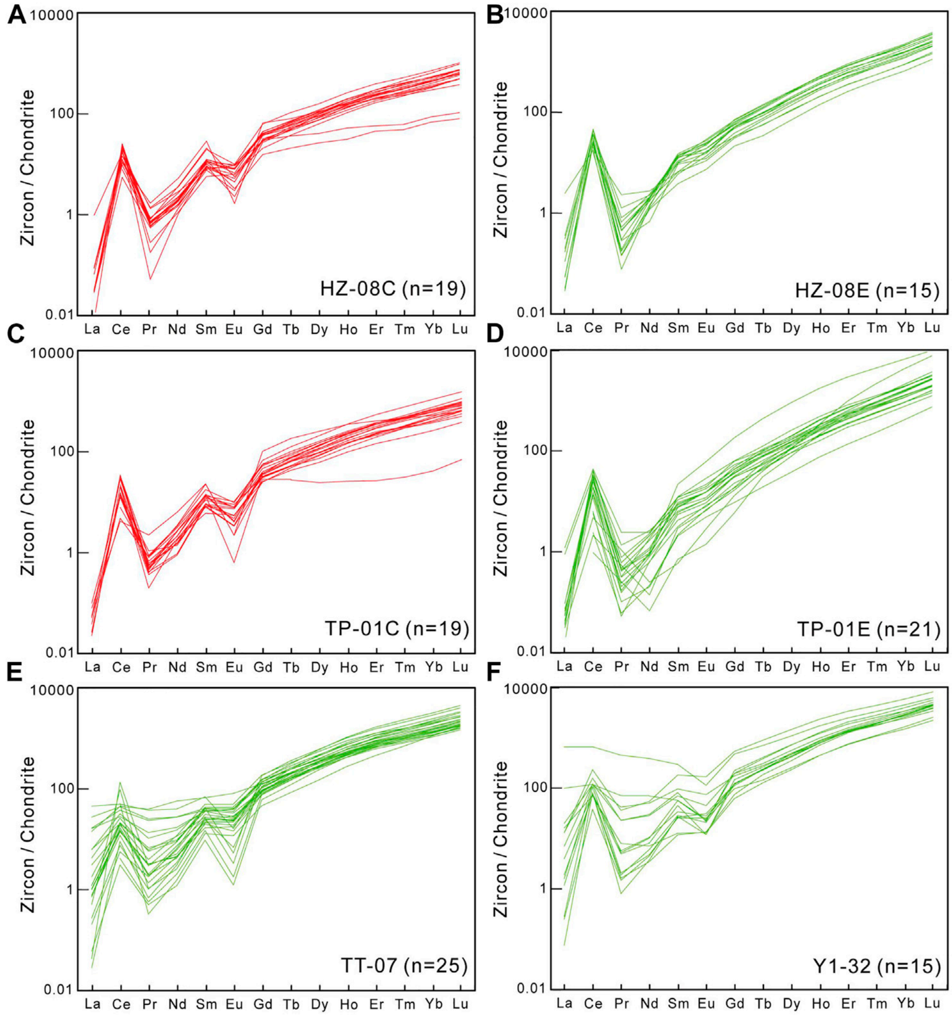

FIGURE 6 | Chondrite-normalized zircon REE patterns for the Huaibei-Linhuan intrusive rock samples: Chondrite normalizing values are from Sun and McDonough (1989).

the zircon trace element compositions. The zircons show in general increasing Yb/Gd with Hf content, which demonstrate a magma cooling and fractionation trend (**Figure 12A**) (Barth and Wooden, 2010). The Cretaceous zircons (or zircon rims) have elevated U/Yb ratio (a proxy of LILE-enrichment), suggesting a more enriched magma source resembling that of typical continental arc (Grimes et al., 2015). This is markedly different from the Precambrian cores, which have lower U/Yb ratio that mimics zircons from typical ocean islands (e.g., Iceland). The Cretaceous and Precambrian zircons have similar Hf and Nb/Yb, showing their host magmas have similar degree of fractionation and alkalinity, respectively (**Figures 12B–C**) (Grimes et al., 2015).

After the magma formation, the lack of distinct Ce or Eu anomalies (some even with weakly positive Eu anomaly), indicates that plagioclase fractionation was insignificant. In the chondrite-normalized REE and primitive mantle-normalized multi-element plots (Sun and McDonough, 1989) (**Figures 9, 13**), the adakitic (quartz-)diorite-granodiorite and the non-adakitic gabbro-dolerite have generally similar arc-type patterns, e.g., LREE enrichments (between EMORB and OIB), HREE depletions (relative to MORB), negative Nb-Ta-Ti anomalies, and positive Pb-Sr anomalies, suggesting that both rock suites were formed in a subduction-related setting. The only difference between them (apart from the adakitic characters such as the Sr-Y contents), i.e., higher LILE and LREE contents for the (quartz-)diorite-granodiorite, is likely attributed to its more fractionated nature compared with the gabbro-dolerite.

Tectonic Evolution of Cretaceous Eastern China

Cretaceous adakitic magmatism in Eastern China has been variably attributed to the progressive decratonization of North China, and/or the Paleo-Pacific subduction and rollback. As discussed in the previous section, our Huaibei-Linhuan (quartz-)diorite-granodiorite samples show geochemical features typical of oceanic slab melting-derived adakites, but

TABLE 3 | Zircon REE contents of plutonic rock samples from the Huaibei-Linhuan coalfield.

Spot no.	La	Ce	Pr	Nd	Sm	Eu	Gd	Tb	Dy	Ho	Er	Tm	Yb	Lu	Y	ΣREE	LREE	HREE	LREE/HREE	(Dy/Yb)N	δEu	δCe	Ce^{4+}/Ce^{3+}
								Ppm															
HZ-08C																							
HZ-08C-01	–	14.96	0.05	0.92	1.74	0.37	8.65	2.61	29.27	10.76	47.17	9.74	88.77	18.48	329	233.50	18.04	215.45	0.08	0.22	0.24	88.37	159.99
HZ-08C-02	0.01	9.89	0.08	1.21	1.81	0.51	5.76	1.67	18.31	6.40	28.73	6.06	55.51	11.96	205	147.91	13.50	134.40	0.10	0.22	0.44	38.94	65.69
HZ-08C-03	–	6.59	0.08	1.01	1.47	0.25	7.27	2.18	21.93	7.65	31.33	6.29	56.77	11.91	224	154.71	9.39	145.32	0.06	0.26	0.19	26.10	53.13
HZ-08C-04	0.01	10.82	0.03	0.50	0.84	0.35	4.06	1.35	15.40	5.70	26.33	5.54	53.64	12.30	175	136.85	12.54	124.32	0.10	0.19	0.48	120.59	262.27
HZ-08C-05	–	11.37	0.00	0.46	1.33	0.13	5.31	1.74	23.98	9.76	47.00	11.06	105.09	23.71	311	240.94	13.30	227.64	0.06	0.15	0.13	756.26	350.01
HZ-08C-06	0.02	10.22	0.05	0.82	1.59	0.54	7.77	2.45	25.88	9.77	43.67	9.03	83.70	17.81	299	213.33	13.24	200.08	0.07	0.21	0.39	50.38	125.96
HZ-08C-07	0.01	7.26	0.05	0.67	1.28	0.34	5.99	1.80	18.48	7.38	31.69	6.82	65.28	14.29	222	161.35	9.62	151.74	0.06	0.19	0.32	39.88	109.37
HZ-08C-08	0.02	7.36	0.07	1.64	3.06	0.31	5.94	1.30	9.93	2.83	9.16	1.50	14.22	2.57	85	59.93	12.47	47.46	0.26	0.47	0.22	28.28	8.83
HZ-08C-09	–	14.12	0.02	0.60	1.12	0.17	6.27	1.76	20.95	8.03	35.89	7.54	72.85	14.94	247	184.25	16.03	168.23	0.10	0.19	0.15	274.83	268.48
HZ-08C-10	0.01	8.50	0.12	1.59	2.87	0.56	12.34	3.81	38.63	14.25	62.24	12.79	117.57	25.08	413	300.36	13.66	286.70	0.05	0.22	0.24	20.26	46.49
HZ-08C-11	0.22	9.77	0.12	1.28	1.16	0.52	7.98	2.13	22.52	8.27	36.94	7.86	72.38	16.46	249	187.62	13.08	174.54	0.07	0.21	0.39	14.65	87.49
HZ-08C-12	0.01	13.61	0.07	0.83	1.64	0.44	8.77	2.54	27.99	10.54	47.25	10.05	86.84	18.18	318	228.75	16.59	212.16	0.08	0.22	0.28	61.99	163.50
HZ-08C-13	0.01	13.12	0.07	0.88	1.35	0.25	7.37	1.88	20.37	7.11	33.32	6.53	60.01	11.99	224	164.26	15.67	148.59	0.11	0.23	0.19	58.53	131.61
HZ-08C-14	0.01	3.21	0.05	0.73	1.73	0.18	3.06	0.75	6.46	1.70	7.16	1.18	11.18	1.95	54	39.35	5.91	33.44	0.18	0.39	0.24	19.22	11.18
HZ-08C-15	0.01	5.71	0.06	0.70	1.22	0.29	5.60	1.97	23.83	8.90	41.57	9.49	89.14	18.33	260	206.82	7.99	198.83	0.04	0.18	0.28	27.58	105.30
HZ-08C-16	0.01	11.99	0.06	0.86	1.84	0.45	7.53	2.10	24.86	9.06	39.23	8.27	76.72	18.22	263	201.20	15.21	186.00	0.08	0.22	0.32	55.59	130.45
HZ-08C-17	0.01	10.47	0.06	0.98	1.27	0.47	8.12	2.26	26.01	9.06	37.88	8.41	73.52	15.60	270	194.10	13.25	180.85	0.07	0.24	0.34	50.64	111.42
HZ-08C-18	–	4.59	0.06	0.91	1.52	0.44	7.92	2.38	26.53	8.54	39.39	7.57	70.85	15.32	274	186.01	7.52	178.50	0.04	0.25	0.31	24.01	46.26
HZ-08C-19	0.02	6.23	0.15	2.37	4.20	0.09	13.03	2.88	27.12	8.41	31.08	5.72	48.46	9.25	250	159.02	13.07	145.95	0.09	0.37	0.03	12.03	9.14
HZ-08E																							
HZ-08E-01	0.08	27.15	0.08	0.97	2.19	1.41	11.84	3.63	48.45	20.94	103.78	23.33	246.61	60.72	631	551.18	31.88	519.30	0.06	0.13	0.68	77.32	498.35
HZ-08E-02	–	11.10	0.01	0.63	2.10	1.31	15.11	5.47	70.42	29.87	148.97	34.75	348.55	84.36	899	752.63	15.14	737.49	0.02	0.14	0.52	492.82	356.96
HZ-08E-03	–	12.49	0.06	1.11	1.88	1.71	14.69	5.21	66.77	27.02	128.31	28.47	283.75	67.04	824	638.53	17.25	621.28	0.03	0.16	0.70	62.74	222.04
HZ-08E-04	0.07	17.18	0.03	0.31	1.44	0.71	6.97	2.13	28.91	11.90	61.77	14.75	157.21	38.94	376	342.33	19.74	322.58	0.06	0.12	0.56	97.24	901.89
HZ-08E-05	–	9.93	0.01	0.55	0.59	0.43	4.47	1.30	18.19	8.22	44.22	11.21	116.65	30.05	263	245.83	11.51	234.32	0.05	0.10	0.58	235.20	483.15
HZ-08E-06	0.01	14.24	0.02	0.58	0.91	0.79	8.10	2.89	40.53	17.43	91.39	22.06	233.01	56.14	559	488.10	16.55	471.55	0.04	0.12	0.60	230.89	691.29
HZ-08E-07	0.01	15.85	0.04	0.97	1.94	1.12	10.00	3.34	43.14	17.88	88.55	20.94	215.69	54.40	567	473.87	19.94	453.93	0.04	0.13	0.63	105.27	293.95
HZ-08E-08	0.01	27.95	0.03	0.88	2.33	1.62	13.70	4.83	67.90	29.53	148.18	36.09	385.16	93.22	919	811.43	32.81	778.62	0.04	0.12	0.68	287.63	698.73
HZ-08E-09	0.04	23.24	0.12	1.05	1.66	1.13	10.85	3.28	49.14	21.27	107.72	26.09	279.51	70.57	690	595.67	27.24	568.43	0.05	0.12	0.61	53.72	520.38
HZ-08E-10	0.05	29.04	0.04	0.80	2.03	0.94	10.86	3.84	49.51	21.25	107.31	26.15	271.91	66.24	665	589.96	32.89	557.07	0.06	0.12	0.49	147.49	711.11
HZ-08E-11	0.03	22.03	0.04	0.91	2.08	1.48	12.22	4.53	64.09	27.74	143.09	35.08	376.34	98.17	899	787.84	26.57	761.27	0.03	0.11	0.70	133.14	593.65
HZ-08E-12	–	17.78	0.02	0.84	1.00	0.64	6.43	2.18	27.73	12.10	60.73	14.77	158.83	41.53	380	344.58	20.27	324.30	0.06	0.12	0.58	316.26	494.85
HZ-08E-13	0.01	14.60	0.05	0.93	1.55	1.39	13.00	4.77	69.21	30.21	158.13	38.87	402.57	103.70	964	838.99	18.53	820.47	0.02	0.12	0.65	84.31	464.34
HZ-08E-14	0.58	10.86	0.22	1.28	1.01	0.98	6.78	2.65	36.00	16.18	82.51	20.98	212.87	55.03	517	447.93	14.94	432.99	0.03	0.11	0.86	7.45	249.61
HZ-08E-15	–	19.01	0.01	0.67	1.52	0.89	10.52	3.71	52.87	22.64	118.81	29.70	318.51	79.79	744	658.65	22.11	636.54	0.03	0.11	0.50	437.25	723.39
TP-01C																							
TP-01C-01	0.01	20.70	0.05	0.75	1.84	0.53	6.60	1.95	19.00	7.09	32.54	7.55	70.92	16.28	222	185.81	23.88	161.93	0.15	0.18	0.41	122.54	237.39
TP-01C-02	0.02	2.61	0.22	3.01	3.57	0.13	5.88	1.04	6.30	1.49	4.47	0.81	7.17	1.79	45	38.52	9.57	28.95	0.33	0.59	0.09	3.58	0.21
TP-01C-03	–	13.72	0.05	1.02	2.17	0.25	7.43	2.46	25.04	9.49	41.57	8.01	79.76	16.20	279	207.18	17.22	189.96	0.09	0.21	0.17	79.36	111.59
TP-01C-04	0.01	8.68	0.11	0.67	1.45	0.32	6.78	2.01	25.03	8.70	38.35	7.89	67.75	14.38	260	182.13	11.23	170.90	0.07	0.25	0.26	24.54	120.33
TP-01C-05	0.01	8.69	0.06	0.72	1.29	0.20	7.69	2.94	33.30	13.34	58.41	12.00	109.08	20.82	407	268.56	10.98	257.58	0.04	0.20	0.15	43.00	155.30
TP-01C-06	–	9.08	0.09	1.59	2.76	0.58	11.77	3.81	41.41	14.64	62.87	12.59	120.78	24.79	424	306.75	14.10	292.65	0.05	0.23	0.26	32.52	50.90
TP-01C-07	–	4.89	0.08	1.66	3.53	0.13	21.18	6.93	65.06	19.89	68.11	11.82	90.07	16.41	592	309.76	10.29	299.46	0.03	0.48	0.04	19.46	14.49
TP-01C-08	–	21.39	0.04	0.46	1.41	0.28	7.80	2.56	29.80	11.83	53.37	11.79	120.19	24.95	378	285.86	23.58	262.29	0.09	0.17	0.21	161.25	595.28
TP-01C-09	0.01	17.73	0.05	0.89	0.94	0.32	5.34	1.62	15.83	5.68	24.31	4.97	45.21	9.78	180	132.69	19.95	112.74	0.18	0.23	0.35	99.20	190.59
TP-01C-10	–	7.76	0.05	1.28	1.71	0.48	11.50	3.23	38.56	13.26	59.19	11.63	104.44	21.49	392	274.57	11.27	263.29	0.04	0.25	0.24	51.25	63.47
TP-01C-11	0.01	12.66	0.04	0.90	1.41	0.46	7.32	2.46	28.44	10.36	50.12	11.13	109.79	22.48	322	257.57	15.48	242.09	0.06	0.17	0.35	94.91	182.99
TP-01C-12	–	19.47	0.05	1.26	2.22	0.47	13.99	4.74	53.42	20.24	90.77	19.86	187.34	39.23	577	453.06	23.47	429.59	0.05	0.19	0.20	112.50	201.16
TP-01C-13	0.02	8.63	0.04	0.43	1.32	0.32	6.37	1.94	22.39	8.35	39.43	8.29	80.68	17.02	251	195.23	10.76	184.47	0.06	0.19	0.28	58.58	212.06
TP-01C-14	0.01	9.58	0.04	1.30	2.06	0.61	10.84	3.49	38.63	13.90	59.56	12.48	114.53	23.18	394	290.21	13.60	276.60	0.05	0.23	0.32	63.82	74.52
TP-01C-15	0.01	7.80	0.07	1.01	1.95	0.47	9.64	2.97	34.44	12.64	58.15	12.37	115.27	24.26	368	281.05	11.31	269.74	0.04	0.20	0.27	33.86	83.10
TP-01C-16	0.01	20.93	0.06	0.74	1.30	0.43	8.30	2.80	35.33	12.76	62.28	13.45	131.41	28.80	419	318.59	23.47	295.12	0.08	0.18	0.30	106.62	425.88
TP-01C-17	–	20.79	0.08	1.49	2.13	0.24	8.28	2.82	30.27	10.72	48.36	10.50	95.14	19.35	331	250.18	24.73	225.45	0.11	0.21	0.15	77.96	133.56
TP-01C-18	–	12.32	0.02	0.85	1.24	0.20	5.22	1.81	21.51	8.43	37.24	8.46	86.21	18.81	261	202.32	14.63	187.70	0.08	0.17	0.20	195.86	190.20
TP-01C-19	0.01	2.99	0.08	1.28	2.09	0.04	7.30	2.41	24.38	8.71	35.39	7.58	64.48	12.81	245	169.55	6.49	163.06	0.04	0.25	0.03	11.03	16.47
TP-01E																							
TP-01E-01	0.01	8.45	0.02	0.41	1.17	0.92	7.75	2.96	38.04	15.62	79.62	19.52	217.36	52.27	513	444.11	10.98	433.13	0.03	0.12	0.70	98.32	450.76
TP-01E-02	–	1.51	0.01	0.10	0.34	0.41	3.49	1.81	29.66	14.90	90.40	24.20	278.40	71.30	479	516.54	2.37	514.17	0.00	0.07	0.73	79.40	827.96
TP-01E-03	0.29	27.41	0.24	1.15	1.91	1.15	13.08	3.93	46.26	19.09	90.32	21.06	220.26	51.56	597	497.70	32.15	465.55	0.07	0.14	0.52	24.02	394.36
TP-01E-04	–	7.23	0.02	0.38	0.66	0.46	4.82	1.62	23.61	9.11	49.72	11.86	131.24	32.25	307	273.00	8.76	264.24	0.03	0.12	0.57	148.91	456.42

(Continued on following page)

TABLE 3 | (*Continued*) Zircon REE contents of plutonic rock samples from the Huaibei-Linhuan coalfield.

Spot no.	La	Ce	Pr	Nd	Sm	Eu	Gd	Tb	Dy	Ho	Er	Tm	Yb	Lu	Y	ΣREE	LREE	HREE	LREE/HREE	(Dy/Yb)N	δEu	δCe	Ce^{4+}/Ce^{3+}
	Ppm																						
TP-01E-05	–	25.44	0.08	1.10	1.86	1.28	11.15	3.39	42.97	17.47	86.01	20.32	213.40	51.49	559	475.96	29.76	446.20	0.07	0.13	0.66	102.23	401.69
TP-01E-06	–	3.57	0.01	0.10	0.32	0.29	2.00	0.73	9.71	4.34	22.89	6.00	71.07	19.32	137	140.34	4.29	136.05	0.03	0.09	0.84	111.16	957.58
TP-01E-07	0.02	18.58	0.05	0.81	1.00	0.64	6.31	2.12	28.58	11.48	60.21	14.80	158.78	37.07	376	340.45	21.10	319.34	0.07	0.12	0.60	104.54	504.57
TP-01E-08	0.01	15.27	0.04	0.45	0.94	0.65	6.66	2.45	32.63	14.22	71.87	18.62	196.49	50.58	454	410.90	17.37	393.53	0.04	0.11	0.58	101.86	848.91
TP-01E-09	–	0.61	0.00	0.03	0.11	0.08	1.23	1.17	19.93	12.21	83.54	23.80	268.62	69.03	450	480.37	0.84	479.53	0.00	0.05	0.43	–	2247.67
TP-01E-10	0.01	19.41	0.04	0.57	1.48	0.90	9.15	3.59	43.20	19.21	99.52	24.37	263.73	67.00	633	552.18	22.42	529.76	0.04	0.11	0.57	125.10	766.01
TP-01E-11	–	11.44	0.03	0.88	1.68	1.06	9.04	3.78	51.29	23.83	123.14	29.62	321.26	82.53	743	659.58	15.09	644.49	0.02	0.11	0.66	114.25	339.23
TP-01E-12	–	3.93	0.01	0.31	0.49	0.49	3.85	1.72	23.81	11.21	57.56	14.52	156.47	41.60	351	315.97	5.23	310.75	0.02	0.10	0.78	238.75	440.81
TP-01E-13	0.02	12.19	0.06	1.01	1.22	0.70	8.26	3.10	39.20	17.33	93.62	22.86	253.57	68.05	573	521.21	15.21	506.00	0.03	0.10	0.50	55.31	328.47
TP-01E-14	0.01	19.73	0.04	0.52	1.39	0.91	10.06	4.14	49.83	23.01	118.63	30.16	330.56	83.54	750	672.53	22.60	649.93	0.03	0.10	0.54	139.33	990.96
TP-01E-15	0.02	2.98	0.00	0.12	0.09	0.17	2.72	1.50	27.96	19.27	163.01	55.32	730.83	200.29	752	1204.28	3.38	1200.90	0.00	0.03	0.42	126.53	6383.18
TP-01E-16	0.01	17.24	0.03	0.43	1.93	1.70	13.34	4.73	66.01	27.55	137.82	32.27	333.98	78.83	868	715.85	21.33	694.52	0.03	0.13	0.75	148.04	804.19
TP-01E-17	–	11.76	0.02	0.47	3.41	3.64	38.25	16.60	233.73	100.03	493.01	113.97	1138.53	255.97	3,055	2,409.39	19.29	2,390.10	0.01	0.14	0.60	220.89	640.44
TP-01E-18	0.01	1.33	0.00	0.07	0.46	0.39	3.97	2.23	34.36	18.54	106.00	29.86	359.25	95.91	602	652.37	2.25	650.12	0.00	0.06	0.60	135.88	1066.29
TP-01E-19	0.22	20.87	0.13	1.26	1.32	0.90	7.47	2.93	34.83	14.96	74.49	18.37	198.78	48.90	474	425.42	24.69	400.73	0.06	0.12	0.69	29.51	372.00
TP-01E-20	0.02	9.41	0.02	0.30	0.86	0.55	6.46	2.01	27.54	11.83	59.79	15.15	159.20	40.93	369	334.07	11.16	322.91	0.03	0.12	0.51	110.29	695.23
TP-01E-21	0.01	24.22	0.06	1.00	1.22	0.90	9.12	3.08	39.68	16.53	78.95	19.41	199.29	49.60	501	443.07	27.41	415.66	0.07	0.13	0.59	116.92	529.71
TT-07																							
TT-07-01	10.65	30.18	3.56	18.45	10.56	0.93	28.04	9.64	112.47	42.32	192.38	39.78	364.68	72.85	1265	936.49	74.33	862.16	0.09	0.21	0.16	1.20	18.66
TT-07-02	0.28	11.60	0.37	5.44	7.52	2.89	38.34	12.15	138.09	50.76	209.53	40.16	347.81	67.11	1488	932.05	28.11	903.94	0.03	0.27	0.42	7.43	22.32
TT-07-03	0.24	8.74	0.30	2.12	3.02	0.84	15.46	5.52	65.78	24.02	108.55	23.36	199.52	41.27	747	498.74	15.26	483.48	0.03	0.22	0.30	6.83	57.82
TT-07-04	3.91	22.91	2.23	12.71	5.71	1.92	18.74	6.23	67.77	25.74	110.77	21.86	194.99	39.81	772	535.29	49.38	485.91	0.10	0.23	0.51	1.88	19.91
TT-07-05	0.42	12.99	0.64	4.45	5.38	2.30	31.60	10.54	119.36	43.25	188.91	37.71	334.76	67.87	1317	860.18	26.18	834.00	0.03	0.24	0.42	5.02	37.66
TT-07-06	3.83	17.14	1.28	7.94	5.47	1.60	18.06	7.19	79.92	30.01	125.96	27.36	230.26	46.38	899	602.41	37.27	565.14	0.07	0.23	0.45	1.89	26.14
TT-07-07	0.06	4.58	0.10	1.58	3.71	0.40	22.76	9.06	116.53	46.05	208.21	44.78	413.87	85.91	1355	957.59	10.42	947.17	0.01	0.19	0.10	11.70	52.81
TT-07-08	0.99	15.91	0.54	4.21	6.58	2.55	27.94	8.97	95.47	33.78	141.69	27.99	247.71	49.89	1034	664.22	30.79	633.43	0.05	0.26	0.49	5.25	36.14
TT-07-09	0.18	7.21	0.13	2.09	2.55	1.02	16.05	5.82	69.92	27.21	115.05	23.49	213.16	45.10	815	528.97	13.18	515.79	0.03	0.22	0.37	11.16	55.13
TT-07-10	1.48	12.46	0.58	5.28	4.18	1.37	19.31	6.50	71.86	27.91	122.39	25.14	220.66	46.78	839	565.90	25.34	540.56	0.05	0.22	0.39	3.31	30.95
TT-07-11	0.05	3.41	0.17	3.02	6.39	0.30	37.25	13.30	152.77	57.79	254.72	53.19	487.39	101.80	1658	1171.57	13.34	1158.23	0.01	0.21	0.05	5.65	15.36
TT-07-12	0.28	12.53	0.18	1.95	3.70	1.40	21.09	7.37	79.73	29.03	123.14	24.56	225.21	44.12	860	574.30	20.06	554.25	0.04	0.24	0.38	13.11	77.55
TT-07-13	0.01	1.88	0.05	0.55	1.45	0.07	12.42	4.42	59.66	23.93	112.95	25.64	247.00	53.68	719	543.73	4.01	539.71	0.01	0.16	0.03	11.07	76.52
TT-07-14	0.72	8.72	0.28	2.36	3.34	1.27	18.34	5.95	72.56	26.45	120.30	25.04	219.95	46.44	808	551.72	16.70	535.03	0.03	0.22	0.39	4.71	51.14
TT-07-15	6.46	26.78	2.39	12.85	6.25	2.33	27.60	9.05	100.46	37.80	163.16	33.68	284.72	58.16	1154	771.69	57.07	714.62	0.08	0.24	0.46	1.67	25.98
TT-07-16	0.12	59.27	0.10	1.19	3.21	1.09	17.71	6.55	83.66	34.70	173.07	39.37	378.63	82.06	1107	880.73	64.98	815.76	0.08	0.15	0.35	125.59	996.26
TT-07-17	0.01	5.50	0.06	1.41	4.08	0.19	30.51	11.50	150.05	59.77	275.09	59.39	538.56	114.13	1745	1250.25	11.25	1239.00	0.01	0.19	0.04	25.60	75.01
TT-07-18	0.17	9.36	0.18	2.82	4.71	1.50	22.05	7.77	89.85	33.76	145.72	29.24	266.15	54.73	1008	668.01	18.73	649.28	0.03	0.23	0.37	11.84	41.56
TT-07-19	1.46	19.45	0.98	7.04	5.62	2.25	25.01	7.57	87.80	31.06	135.34	27.15	233.51	47.37	960	631.61	36.81	594.80	0.06	0.25	0.49	3.85	30.52
TT-07-20	0.00	2.52	0.05	0.93	2.26	0.10	15.54	5.41	72.71	28.34	135.10	28.02	257.41	55.51	837	603.91	5.87	598.04	0.01	0.19	0.04	14.67	49.21
TT-07-21	3.35	27.20	3.72	26.52	10.14	4.68	25.91	7.79	84.65	30.09	131.21	26.06	230.72	48.04	945	660.08	75.61	584.48	0.13	0.25	0.84	1.67	8.83
TT-07-22	0.01	82.42	0.28	4.07	6.15	2.06	30.87	9.02	98.91	38.17	168.06	35.43	325.58	69.40	1141	870.43	94.98	775.45	0.12	0.20	0.37	90.94	248.14
TT-07-23	0.23	8.47	0.30	2.05	3.72	1.66	16.90	5.84	64.80	23.69	102.01	20.70	179.62	37.32	731	467.32	16.44	450.88	0.04	0.24	0.54	6.61	46.43
TT-07-24	0.18	10.27	0.19	3.41	3.93	1.33	21.18	7.56	90.00	33.82	149.86	31.27	289.42	60.86	1045	703.29	19.31	683.98	0.03	0.21	0.36	12.19	45.83
TT-07-25	–	31.35	0.03	0.71	1.96	0.67	9.40	3.09	37.51	15.61	74.85	17.74	188.52	43.40	498	424.85	34.72	390.12	0.09	0.13	0.40	318.95	794.77
Y1-32																							
Y1-32-01	161.08	416.78	44.06	186.02	46.60	6.78	100.76	27.05	283.89	100.74	422.50	87.14	788.51	162.68	2,890	2,834.58	861.31	1973.27	0.44	0.24	0.29	1.19	9.95
Y1-32-02	0.07	67.75	0.20	2.28	4.00	1.49	25.91	9.17	122.91	51.43	246.01	56.06	542.96	120.67	1581	1250.91	75.79	1175.12	0.06	0.15	0.34	92.52	379.76
Y1-32-03	4.84	73.66	4.09	24.11	15.13	4.43	36.91	10.81	121.66	45.73	231.03	50.71	512.06	111.36	1506	1246.54	126.27	1120.28	0.11	0.16	0.55	3.79	20.44
Y1-32-04	0.06	23.88	0.14	2.15	4.13	1.85	25.24	9.20	112.42	46.58	221.15	45.95	447.76	100.51	1414	1041.03	32.22	1008.81	0.03	0.17	0.43	44.45	121.28
Y1-32-05	0.28	46.96	0.18	2.88	4.50	1.24	26.33	8.71	113.27	46.74	220.69	51.39	514.13	114.11	1466	1151.41	56.04	1095.37	0.05	0.15	0.27	49.21	190.57
Y1-32-06	–	47.65	0.16	1.66	1.85	0.80	15.75	7.11	91.18	41.47	213.38	49.78	507.79	118.28	1319	1096.85	52.11	1044.75	0.05	0.12	0.31	93.81	592.76
Y1-32-07	3.15	146.11	3.53	26.08	28.64	10.01	113.66	34.44	381.02	136.38	573.48	115.30	1031.31	214.52	3,890	2,817.62	217.52	2,600.10	0.08	0.25	0.47	9.46	32.00
Y1-32-08	0.46	45.06	0.48	3.87	7.09	0.71	31.02	10.12	128.59	49.53	223.48	47.67	424.37	88.99	1484	1061.43	57.66	1003.77	0.06	0.20	0.12	21.10	90.78
Y1-32-09	0.96	48.87	0.55	5.04	5.32	1.67	23.69	9.01	108.15	45.51	223.03	50.22	491.74	111.83	1430	1125.59	62.41	1063.18	0.06	0.15	0.38	16.22	110.69
Y1-32-10	3.14	99.25	2.23	13.64	10.99	2.68	41.13	11.84	145.91	57.46	266.53	60.29	593.09	132.37	1746	1440.54	131.93	1308.62	0.10	0.16	0.34	8.83	60.95
Y1-32-11	3.93	44.28	0.77	3.38	2.00	0.78	13.10	4.90	60.46	25.82	127.95	29.27	289.36	66.97	834	672.98	55.14	617.84	0.09	0.14	0.35	5.86	198.41
Y1-32-12	0.38	76.54	0.51	4.85	8.87	1.35	41.55	14.74	186.84	74.20	352.79	73.74	693.09	147.27	2,206	1676.73	92.50	1584.23	0.06	0.18	0.18	36.06	146.58
Y1-32-13	1.69	76.02	2.24	14.35	12.81	1.29	47.24	15.62	189.25	71.07	319.73	66.42	594.76	121.24	2,156	1533.73	108.40	1425.33	0.08	0.21	0.14	8.10	38.23
Y1-32-14	0.02	50.95	0.08	1.79	4.28	0.71	26.08	9.16	122.28	49.43	237.06	52.25	475.26	103.53	1474	1132.88	57.83	1075.05	0.05	0.17	0.16	186.27	309.75
Y1-32-15	24.22	74.34	6.92	33.44	9.00	1.43	20.58	5.55	66.00	25.96	125.12	28.32	260.78	58.05	805	739.71	149.35	590.36	0.25	0.17	0.31	1.39	15.13

*$\delta Eu = (2\times Eu_N)/(Sm_N + Gd_N)$; $\delta Ce = (2\times Ce_N)/(La_N + Pr_N)$.

TABLE 4 | | Major and trace element compositions of plutonic rock samples from the Huaibei-Linhuan coalfield.

Sample no.	TP-01	TP-04	HZ-08	HZ-13	YL-03	YL-07	TT-07	TT-12	Y1-29	Y1-32	Y2-08	Y2-23
Lithology	diorite	diorite porphyry	Diorite	Diorite	diorite porphyry	diorite porphyry	microgabbro	microgabbro	dolerite	dolerite	dolerite	dolerite
SiO2	58.2	61.27	58.81	59.3	60.42	57.45	50.54	50.88	48.06	43.85	48.59	42.58
TiO2	0.61	0.35	0.54	0.53	0.47	0.57	0.77	0.71	1.33	0.9	0.89	0.85
Al2O3	16.12	14.53	14.62	14.53	14.68	14.59	13	12.22	14.25	14.39	14.55	14.23
Fe2O3	6.19	4	6.71	6.67	5.53	6.05	6.99	7.49	14.68	13.72	10.15	10.46
MnO	0.08	0.06	0.06	0.06	0.09	0.09	0.06	0.1	0.19	0.24	0.12	0.12
MgO	4.04	2.87	4.58	4.63	4.2	4.52	6.43	6.73	6.76	8.63	5.69	5.44
CaO	5.6	4.17	5.53	5.52	3.54	3.48	6.78	8.83	7.38	9.55	6.88	11.82
Na2O	4.3	6.8	4.34	4.37	5.11	4.74	2.08	2.63	3.35	2.45	3.16	2.77
K2O	2.33	2.35	2.11	2.2	2.12	2.05	0.57	0.83	0.22	0.17	0.92	0.52
P2O5	0.2	0.12	0.17	0.17	0.14	0.16	0.2	0.19	0.2	0.14	0.29	0.26
LOI	1.87	2.9	1.82	1.54	3.69	5.83	12.36	8.96	3.19	5.71	8.63	10.19
Total	99.53	99.41	99.29	99.52	99.98	99.53	99.77	99.57	99.61	99.73	99.86	99.23
Sc	16.33	10.12	18.68	17.00	15.21	15.54	21.68	20.29	31.91	23.91	20.84	19.13
V	121.2	65.00	128.0	115.9	96.23	102.8	168.0	157.1	211.3	148.7	130.2	119.8
Cr	129.5	137.5	244.4	220.4	194.4	210.0	472.2	467.3	162.6	190.4	192.8	324.2
Co	16.82	11.71	24.38	21.91	17.05	18.09	36.02	35.17	41.84	51.24	39.91	41.36
Ni	49.19	66.20	104.2	93.54	57.45	73.21	200.7	216.2	86.12	144.7	141.9	192.8
Cu	3,365	3,933	7,265	5,984	1768	4,103	1108	1629	76.04	68.44	6516	749.6
Zn	2,132	2,402	4,520	3,720	1095	2,408	687.7	1002	126.60	81.50	4,270	526.1
Ga	21.36	20.43	18.24	18.08	19.10	20.01	17.11	16.40	18.96	17.27	18.55	17.40
Ge	1.36	1.06	1.42	1.32	0.91	1.41	1.81	1.33	1.47	1.39	1.38	2.03
Rb	56.44	48.12	36.97	44.70	50.95	48.62	9.97	14.40	5.89	4.08	16.03	8.49
Sr	773.6	826.5	684.2	1041	680.3	677.7	766.7	975.0	368.2	384.2	740.0	847.7
Zr	120.5	71.52	82.98	83.33	114.4	115.4	87.15	82.57	77.29	53.40	113.1	100.1
Nb	6.06	3.47	3.95	3.52	4.60	5.07	3.98	3.79	4.07	2.87	9.45	8.81
Cs	1.96	2.36	0.91	1.14	0.57	0.63	0.80	0.56	0.32	0.30	0.27	0.20
Ba	1060	1082	955.2	1071	1215	2,264	472.9	641.1	316.6	243.6	749.9	765.6
Hf	3.21	2.15	2.33	2.20	3.09	3.12	2.27	2.16	2.14	1.49	2.56	2.33
Ta	0.35	0.20	0.23	0.21	0.30	0.32	0.24	0.24	0.23	0.16	0.48	0.45
Pb	153.4	237.4	321.2	275.5	113.1	220.5	49.77	70.93	26.14	3.17	285.1	65.93
Th	4.92	2.25	3.54	3.48	4.54	4.97	2.66	2.51	1.57	1.08	7.60	7.16
U	1.36	1.20	1.24	1.21	1.41	1.59	1.00	0.96	0.30	0.22	1.51	1.47
La	22.09	9.54	18.38	15.71	16.76	18.05	13.30	13.07	15.23	11.29	43.59	40.52
Ce	45.13	19.29	36.41	31.07	32.53	35.15	28.42	27.33	31.81	23.53	84.14	77.94
Pr	5.49	2.44	4.47	3.90	3.98	4.25	3.75	3.59	4.00	2.97	9.32	8.66
Nd	22.66	10.24	18.58	16.17	16.03	17.44	16.32	15.54	16.91	12.52	34.02	31.59
Sm	4.43	2.12	3.66	3.22	3.28	3.48	3.45	3.33	3.73	2.81	5.37	4.93
Eu	1.44	0.87	1.19	1.14	1.14	1.50	1.04	1.10	1.23	1.02	1.55	1.46
Gd	4.47	2.17	3.65	3.23	3.30	3.65	3.48	3.31	4.15	3.12	5.99	5.61
Tb	0.57	0.27	0.47	0.41	0.43	0.46	0.46	0.44	0.72	0.54	0.67	0.62
Dy	2.96	1.43	2.46	2.19	2.28	2.45	2.48	2.34	4.58	3.41	3.50	3.26
Ho	0.57	0.28	0.48	0.42	0.44	0.47	0.46	0.44	0.93	0.70	0.68	0.64
Er	1.66	0.83	1.39	1.24	1.30	1.36	1.32	1.24	2.72	2.02	1.99	1.90
Tm	0.23	0.12	0.20	0.18	0.19	0.19	0.18	0.17	0.40	0.29	0.27	0.26
Yb	1.53	0.79	1.24	1.15	1.22	1.28	1.15	1.09	2.56	1.88	1.75	1.66
Lu	0.23	0.12	0.19	0.18	0.19	0.19	0.17	0.16	0.39	0.29	0.26	0.26
Y	15.48	7.73	13.29	11.74	12.19	12.73	12.44	11.72	24.13	18.27	17.78	17.04
ΣREE	113.45	50.51	92.77	80.22	83.05	89.92	75.98	73.14	89.34	66.38	193.1	179.32
LREE	101.23	44.5	82.69	71.22	73.71	79.87	66.28	63.95	72.9	54.14	177.98	165.11
HREE	12.22	6.01	10.08	9	9.34	10.05	9.7	9.18	16.44	12.24	15.11	14.22
LREE/HREE	8.28	7.41	8.21	7.91	7.89	7.95	6.84	6.96	4.44	4.42	11.78	11.61
(La/Yb)N	10.36	8.63	10.62	9.77	9.84	10.13	8.33	8.61	4.27	4.31	17.85	17.5
(Dy/Yb)N	1.93	1.81	1.98	1.9	1.87	1.91	2.16	2.15	1.79	1.81	2	1.96
δEu	0.98	1.23	0.98	1.07	1.05	1.27	0.91	1	0.95	1.05	0.83	0.85
δCe	0.98	0.96	0.96	0.95	0.94	0.95	0.97	0.96	0.98	0.97	0.98	0.97

also contain Precambrian inherited zircon core (Haizi: 2,475 ± 33 Ma; Taiping: 2,463 ± 23 Ma) that reflect NCC crustal inheritance (Cenozoic Nushan basalt: ca. 2,455 and 2,716 Ma) (Ping et al., 2019). An oceanic slab-melting model was also proposed for the adakites (some high-Mg) in the nearby Banjing pluton (Xuhuai area), which is slightly younger (zircon U-Pb: 126.4 ± 2.1 Ma) and has similar structural setting (proximal to the Tanlu fault) to the Huaibei-Linhuan adakites

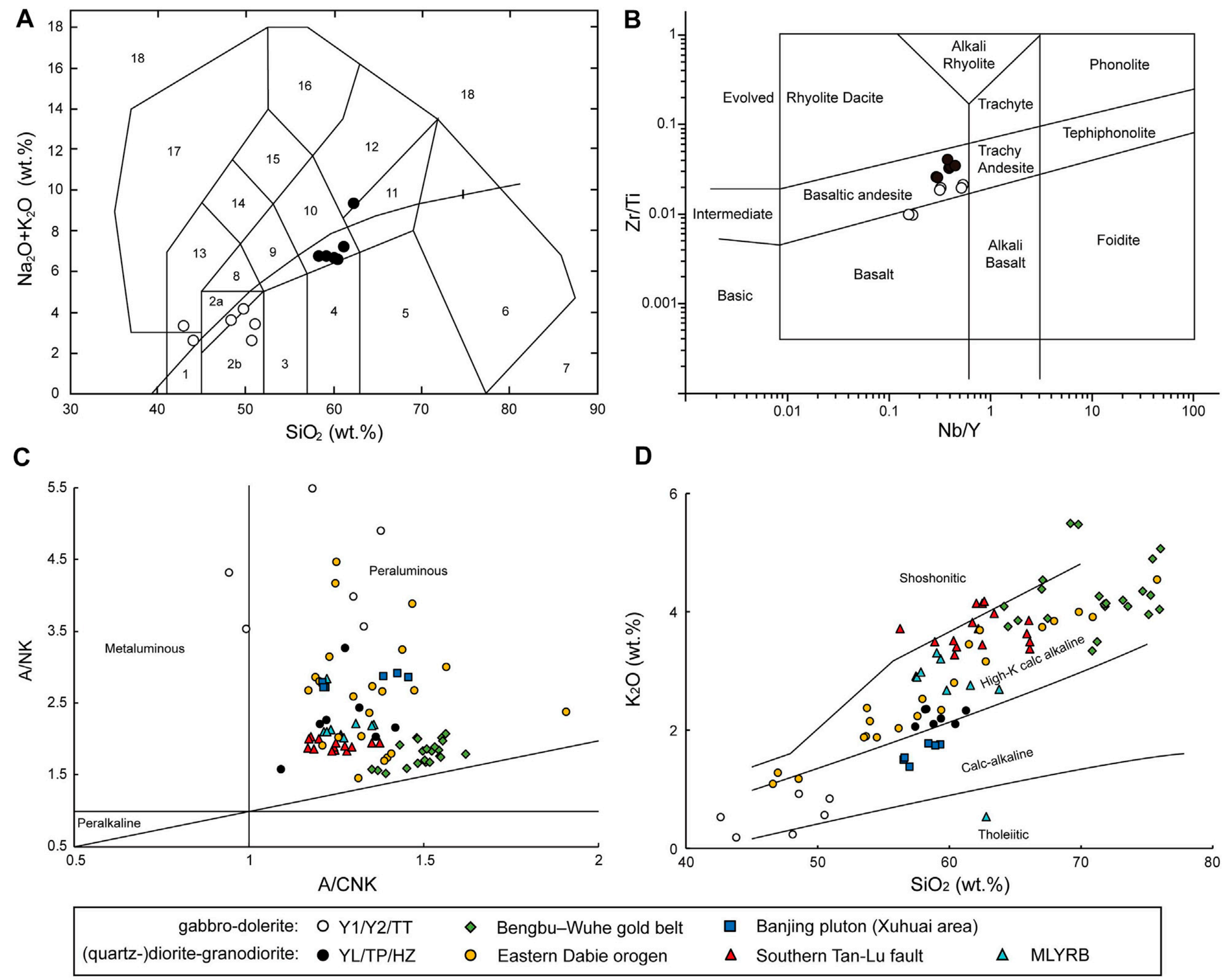

FIGURE 7 | Petrological classification plots for the igneous rock samples from the Huaibei-Linhuan coalfield: **(A)** Total Alkali Silica (TAS) (base map after Middlemost, 1994). The curve denotes the Ir (Irvine) boundary, separating the alkaline (above) and sub-alkaline (below). Number: 1) olivine gabbro; 2a) alkaline gabbro; 2b) sub-alkaline gabbro; 3) gabbroic diorite; 4) diorite; 5) granodiorite; 6) granite; 7) quartzolite; 8) monzogabbro; 9) monzodiorite; 10) monzonite; 11) quartz monzonite; 12) syenite; 13) foid gabbro; 14) foid monzogabbro; 15) foid monzosyenite; 16) foid syenite; 17) foidolite; 18) tawite/urtite/italite; **(B)** Zr/Ti vs. Nb/Y (after Pearce, 1996); **(C)** A/NK vs. A/CNK (base map after Maniar and Piccoli, 1989); **(D)** K_2O vs. SiO_2 (after Peccerillo and Taylor, 1976). For **Figures 5–6, 9–10**, data from the adakitic rocks in the Bengbu-Wuhe gold belt (Li C. et al., 2020), Banjing pluton (Zhou et al., 2019), Eastern Dabie Orogen (Zhang et al., 2013), Lower Yangtze River Belt (Liu S.-A. et al., 2010) and southern Tanlu fault (Liu S.-A. et al., 2010) are also shown for comparison.

(Zhou et al., 2019). The Huaibei-Linhuan and Banjing are geochemically similar in terms of their low Th content and low Rb/Y and Nb/Y ratios (suggestive of minor crustal melt-derived enrichment), which are in marked contrast with the thickened lower crust-derived Bengbu-Wuhe gold ore-forming granitoids (Liu S.-A. et al., 2010) (**Figures 10C–D**).

Although not without controversies, many studies suggest that the Tanlu fault zone was first formed as a Triassic-Jurassic syn-collisional sinistral fault between the North China and South China (phengite Ar-Ar: ca. 221–210 and 198–181 Ma) (Zhu et al., 2009), and had displaced the Dabie–Sulu UHP metamorphic belt across a ~500 km distance (Zhu et al., 2005). The fault (esp. the southern part where the Huaibei-Linhuan coalfield is located) has likely reactivated several times during the Early Cretaceous (e.g., hornblende Ar-Ar = 143.3 Ma; phengite Ar-Ar = 138.8 Ma) (Zhu et al., 2005). The sinistral movement in the southern Tanlu fault (138.8 Ma; Zhu et al., 2005) was accompanied (or soon followed) by emplacement of granodiorite (~131 Ma), diorite (~130 Ma), and lamprophyre dykes (~128 Ma) of the Guandian intrusive complex (Zhao et al., 2020), whose ages are largely coeval (within error) with the ca. 130–129 Ma ages obtained for the Huaibei-Linhuan (quartz-)diorite-granodiorite. Based on whole-rock geochemical and Sr-Nd isotope geochemical data, Zhao et al. (2020) suggested that these Early Cretaceous intrusive rocks at Guandian were formed in an extensional setting, possibly related to the Paleo-Pacific subduction rollback. Such tectonic setting would fit with our suggestion that the Huaibei-Linhuan high-Mg adakitic (quartz-)diorite-granodiorite was formed by partial melting of the

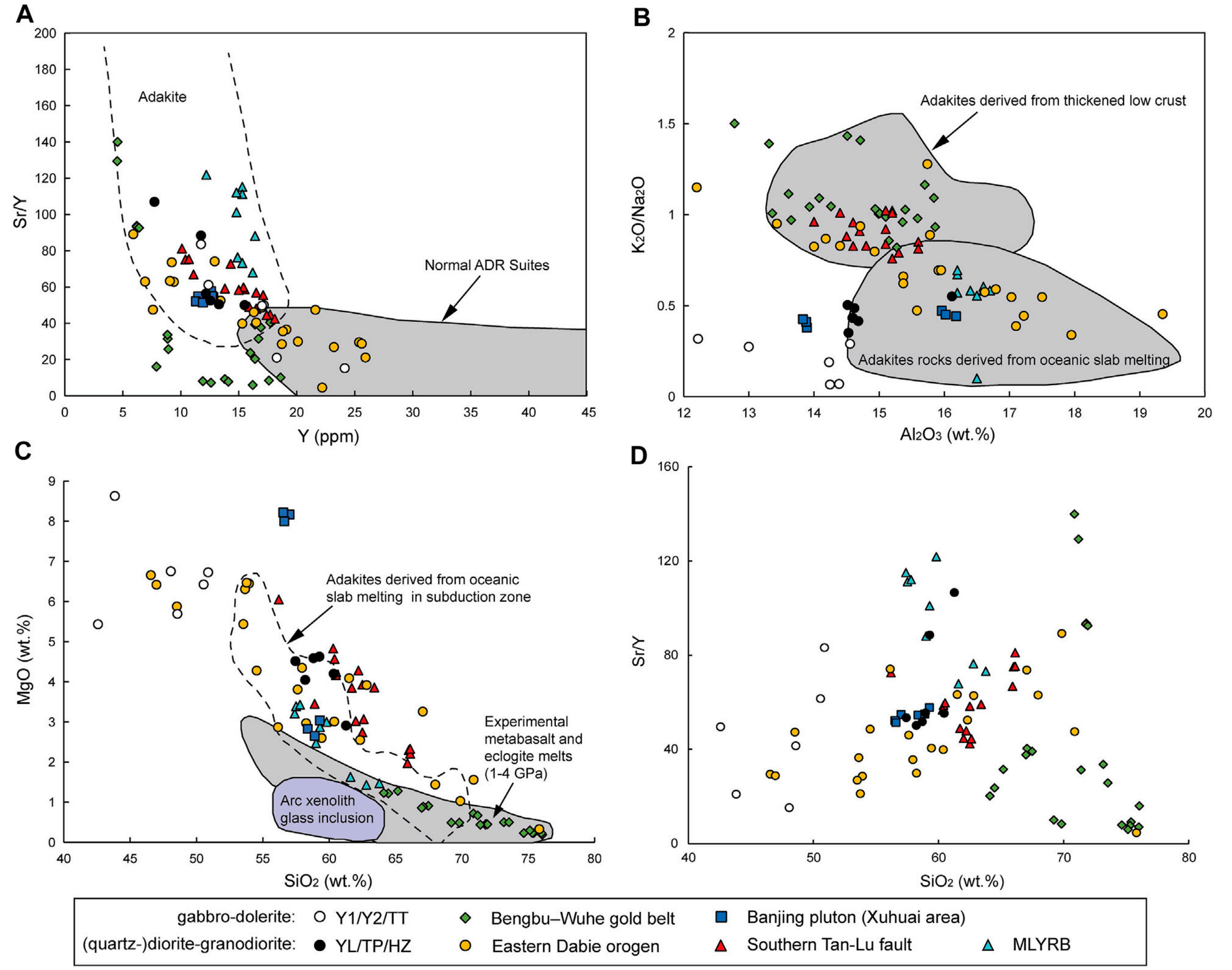

FIGURE 8 | Adakite discrimination plots for the igneous rock samples from the Huaibei-Linhuan coalfield: **(A)** Sr/Y vs. Y (after Defant and Drummond, 1993), andesites, dacites and rhyolites (ADR); **(B)** K_2O/Na_2O vs. Al_2O_3 (after Liu et al., 2010a, and ref. therein); **(C)** MgO vs. SiO_2 (base map after Liu et al., 2010a, and ref. therein); **(D)** Sr/Y vs. SiO_2 (after Richards et al., 2012).

subducted slab. A slab-tearing may also be possible (Zhao et al., 2016) to generate the adakites, although more work will be needed to constrain when and how it actually took place.

A detailed review of the Early Cretaceous tectonics across the North Pacific by Liu et al. (2021) has revealed that the Eastern Eurasia, as facilitated by the Paleo-Pacific subduction rollback (*via* eastward migration of the shallow mantle convection system), has undergone three major extensional events at around 160–145 Ma, 135–120 Ma (peak), and post-120 Ma. These extensional events were accompanied by synextensional magmatism at around 160 Ma, 130–120 Ma (magmatic flare-up), and 100–80 Ma. It is thus clear that the Huaibei-Linhuan high-Mg adakitic magmatism, like many Cu-Au ore-fertile or ore-barren adakitic rocks in the southern Tanlu fault and the LMYRB, were formed during this 130–120 Ma magmatic flare-up during the peak extension episode. Meanwhile, the late-Early Cretaceous gabbro-dolerite magmatism in Huaibei-Linhuan (Qingdong: 115.8 Ma; Yuandian-1: 105.8 Ma) was formed in the post-peak extension. The highly attenuated North China continental crust around the southern Tanlu fault may have enabled higher degree of partial melting with lower degree of crustal assimilation and fractionation, thereby forming more mafic rocks in Huaibei-Linhuan. The presence of highly-attenuated crust is also supported by the complete absence of inherited zircon core or xenocrystic zircon in the Huaibei-Linhuan gabbro-dolerite.

Metallogenic Implications in Fertile *Versus* Barren Adakites

From a metallogenic perspective, it is still unclear on why some Early Cretaceous adakites in Eastern China are Cu-Au ore-fertile (e.g., those in the MLYRB), whereas some others are ore-barren (e.g., those along the southern Tanlu fault). Based on whole-rock elemental and Sr-Nd-Pb isotope data, Liu S.-A. et al. (2010) argued that the ore-fertile MLYRB adakites were formed from partial

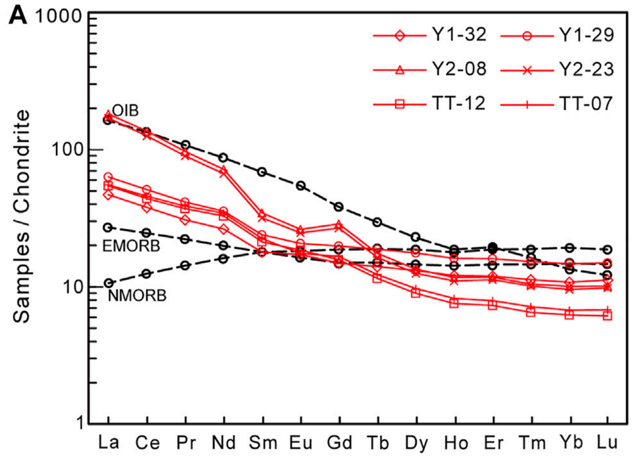

FIGURE 9 | Chondrite-normalized whole-rock REE patterns for the Huaibei-Linhuan intrusive rock samples: **(A)** gabbro-dolerite; **(B)** (quartz-)diorite and granodiorite. Chondrite normalizing values are from Sun and McDonough (1989).

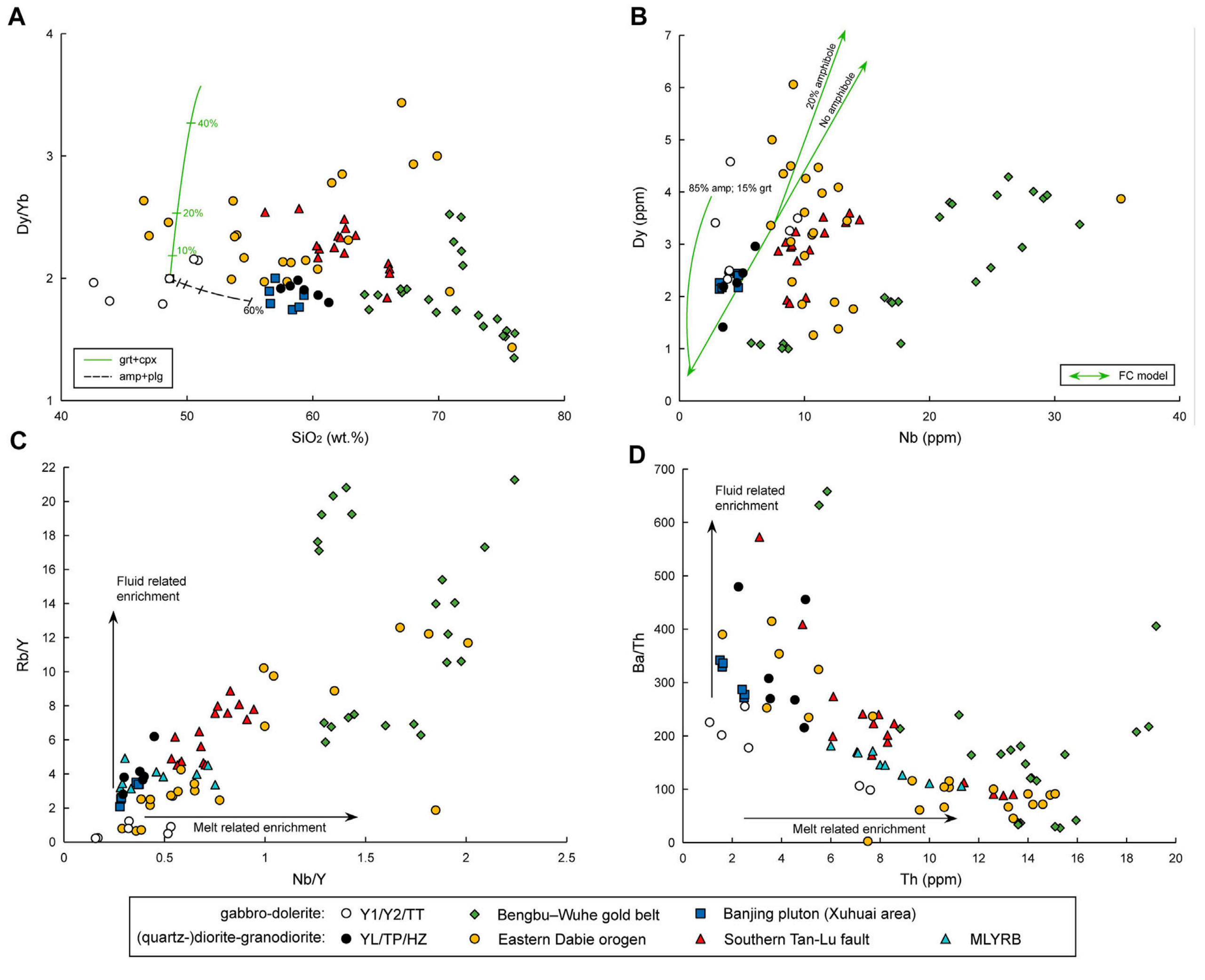

FIGURE 10 | (A–B) Trace element plots for identifying amphibole–garnet fractionation: **(A)** Dy/Yb vs. SiO_2. Model fractionation paths are from Davidson et al. (2007), Macpherson (2008); **(B)** Dy vs. Nb; **(C)** Nb/Ta vs. Nb. Fractional crystallization (FC) and assimilation-fractional crystallization (AFC) trends are from Gómez-Tuena et al. (2007); **(C–D)** Trace element plots for differentiating fluid-related vs. melt-related enrichments (after Zhao et al., 2020): **(C)** Rb/Y vs. Nb/Y; and **(D)** Ba/Th vs. Th. Abbreviations: amp = amphibole; cpx = clinopyroxene; grt = garnet, pl = plagioclase.

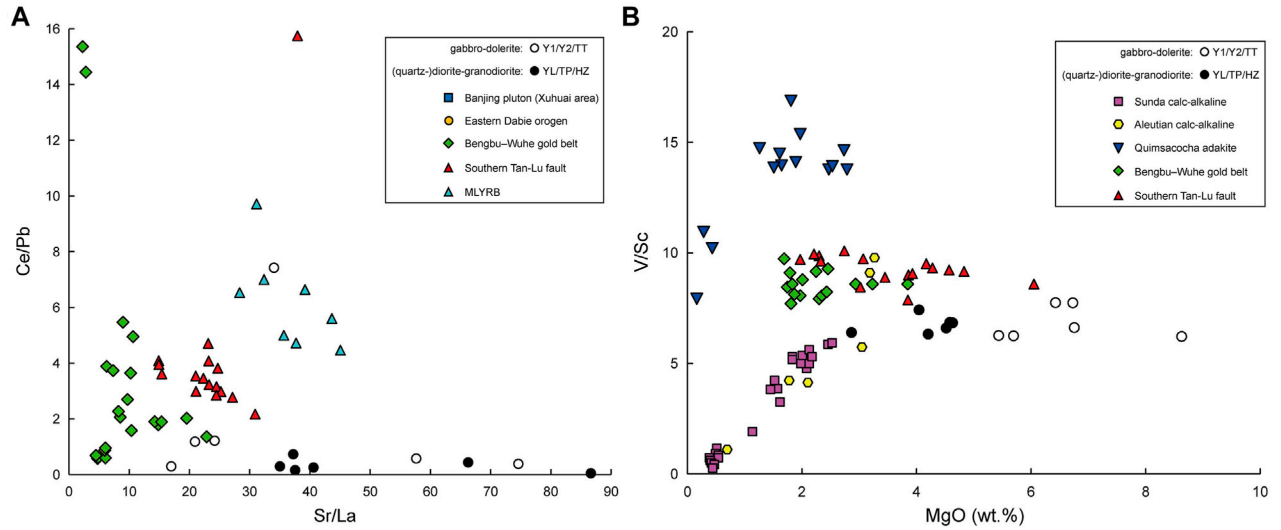

FIGURE 11 | Petrogenetic discrimination plots for the Huaibei-Linhuan intrusive rock samples: **(A)** Ce/Pb vs. Sr/La (after Liu S.-A. et al., 2010); **(B)** V/Sc vs. MgO (after Lee et al., 2005; Kamvong et al., 2014). V/Sc = proxy for fO_2 of parental magma. Data from the ore-related porphyries from Quimsacocha (Ecuador) (Beate et al., 2001) and Dexing (Eastern China) (Wang et al., 2006) and ore-barren calc-alkaline rocks from the Sunda arc (Reubi and Nicholls, 2004) and Aleutian arc (Jicha and Singer, 2006) are also shown for comparison.

melting of the seawater-metasomatized Paleo-Pacific slab, whereas the ore-barren adakites along the southern Tanlu fault were derived from the delaminated North China eclogitic lower continental crust. This explanation, however, is unlikely applicable to the ore-barren Huaibei-Linhuan adakitic (quartz-)diorite-granodiorite, as their formation was likely slab-melting-related similar to the MLYRB adakites. This suggestion is supported by the elevated Sr/La values, which are comparable to the ore-fertile MLYRB adakites but considerably higher than the ore-barren adakites along the southern Tanlu fault (**Figure 12A**).

Porphyry-type Cu-Au fertility is controlled by a number of factors, including the contents of metals, water and sulfur of the magma, the magma oxygen fugacity (fO_2), as well as thickness of the crust into which the magma was emplaced (e.g., Audétat et al., 2008; Richards et al., 2012; Park et al., 2019, 2021). Comparing with our Huaibei-Linhuan samples, both the mineralized adakites in the MLYRB and the barren adakites in the southern Tanlu fault are more fractionated (Liu S.-A. et al., 2010) (**Figure 7D**). The MLYRB adakites have distinctly higher Sr/Y (67.96–121.89) than their barren counterparts in Huaibei-Linhuan (15.26–106.95) and the southern Tanlu fault (42.49–81.19). The "more-adakitic" (higher Sr/Y) character in the MLYRB rocks may have caused by the higher magma water content (i.e., "wetter magma"), which can suppress plagioclase fractionation and promote early amphibole ± garnet fractionation (Richards, 2011, and ref. therein).

Previous studies suggested that elevated zircon Eu/Eu* (>0.3) can reflect elevated magma water content, as widely reported from ore-forming porphyries at El Salvador and Chuquicamata-El Abra (Chile), Yanacocha (Peru), Yerington (Nevada, US), Batu Hijau (Indonesia), Tampakan (Philippines), and Dexing, Qulong, and Jiama (China) (Ballard et al., 2002; Dilles et al., 2015; Lu et al., 2016). Lu et al. (2016) proposed that wet fertile magmas have commonly high 10,000*(Eu/Eu*)/Y and Eu/Eu* ratios, with both ratios being positively correlated with (Ce/Nd)/Y. Zircon Ce/Nd ratio can be used as a proxy of magma fO_2 in replace of Ce^{4+}/Ce^{3+}, which is hard to be accurately determined due to the very low (often below the detection limit) zircon La and Pr contents, and the zircon La content is also susceptible to contamination by minute apatite inclusions (Lu et al., 2016; Loucks et al., 2020). Yttrium is added to the denominator of 10,000*(Eu/Eu*)/Y and (Ce/Nd)/Y because its content is commonly low in fertile magmas, caused probably by early hornblende fractionation (Lu et al., 2016, and ref. therein).

From **Figures 14A–B**, it is seen that the Cretaceous Huaibei-Linhuan adakites have comparable 10,000*(Eu/Eu*)/Y and Eu/Eu* ratios to those of the ore-forming granodiorite porphyries in the MLYRB (Jiurui orefield; Xu et al., 2021), as well as to many other fertile adakitic suites (Lu et al., 2016). Similar to the MLYRB ore-forming porphyries, the zircon 10,000*(Eu/Eu*)/Y and Eu/Eu* ratios of the Huaibei-Linhuan adakites are correlated positively with (Ce/Nd)/Y. This suggests that the Huaibei-Linhuan adakitic magma was not H_2O-poor, as also supported by the considerable amount of hornblende present in our samples (**Figure 14C**).

Therefore, we considered that the cause of Cu-Au infertility for the Huaibei-Linhuan adakites may lie in the lower fO_2 of their parental magma. In **Figure 14**, the Huaibei-Linhuan adakites have generally lower (Ce/Nd)/Y (avg. 0.035) than their MLYRB counterpart (avg. 0.051), suggesting lower fO_2 in the former. For the case of Huaibei-Linhuan, the Ce/Nd ratio can serve as good proxy for the Ce anomaly, as indicated by certain positive correlation (R^2 = 0.29) between the two (**Figure 14D**). The more reducing nature of the Huaibei-Linhuan adakitic magma is further supported by the whole-rock V/Sc content, which serves as a proxy for the original magma fO_2 (Lee et al., 2005). In the V/Sc vs. Mg discrimination plot (**Figure 11B**), the Huaibei-Linhuan adakites have distinctly lower V/Sc values than the Cu-Au ore-related porphyries from Quimsacocha (Ecuador) (Beate et al., 2001) and

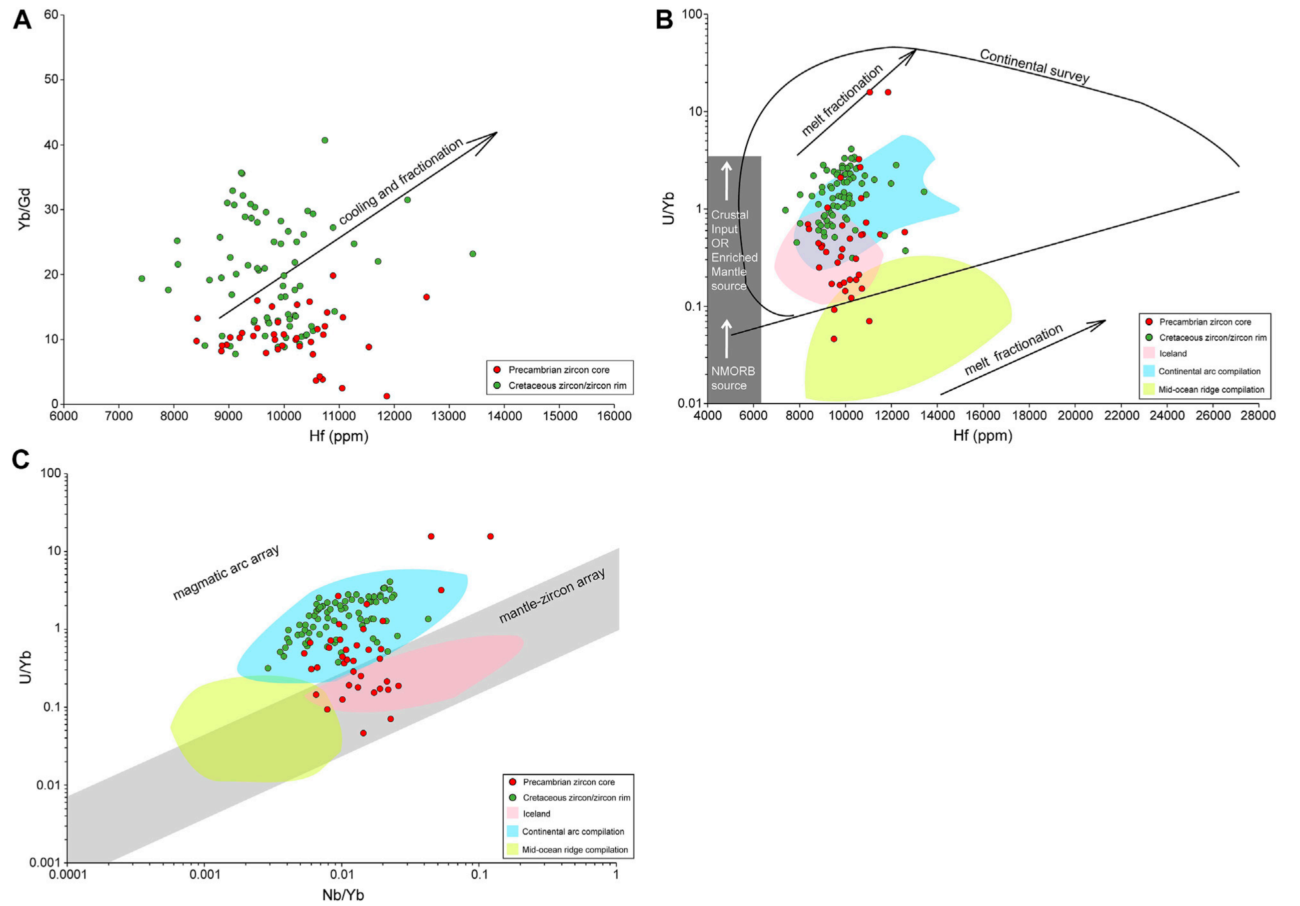

FIGURE 12 | Plots of **(A)** Yb/Gd vs. Hf (base map from Barth and Wooden, 2010), **(B)** U/Yb vs. Hf (base map from Grimes et al., 2015), and **(C)** U/Yb vs. Nb/Yb (base map from Grimes et al., 2015) for zircons from the Huaibei-Linhuan intrusive rock samples.

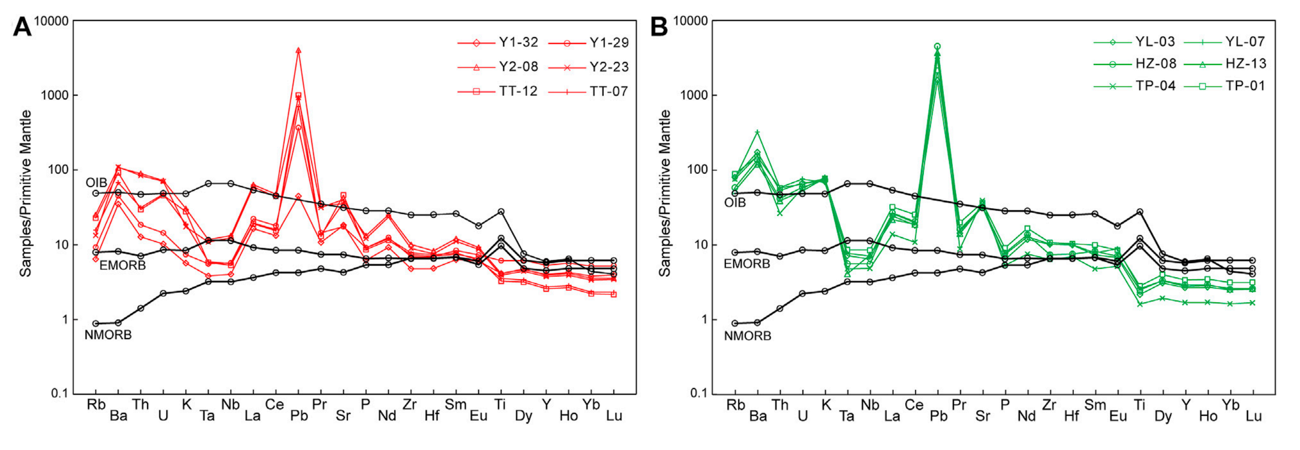

FIGURE 13 | Primitive mantle-normalized spider diagrams for the Huaibei-Linhuan intrusive rock samples: **(A)** gabbro-dolerite; **(B)** (quartz-)diorite and granodiorite. Primitive mantle normalizing values are from Sun and McDonough (1989).

Dexing (Eastern China) (Wang et al., 2006). The V/Sc values remain constant with decreasing MgO, indicating that the V/Sc is not dependent on fractionation. Elevated magma fO_2 has been suggested to be critical in forming porphyry-style Cu-Au mineralization, as it would inhibit early sulfide crystallization and allow chalcophile metals to concentrate in late-stage hydrothermal

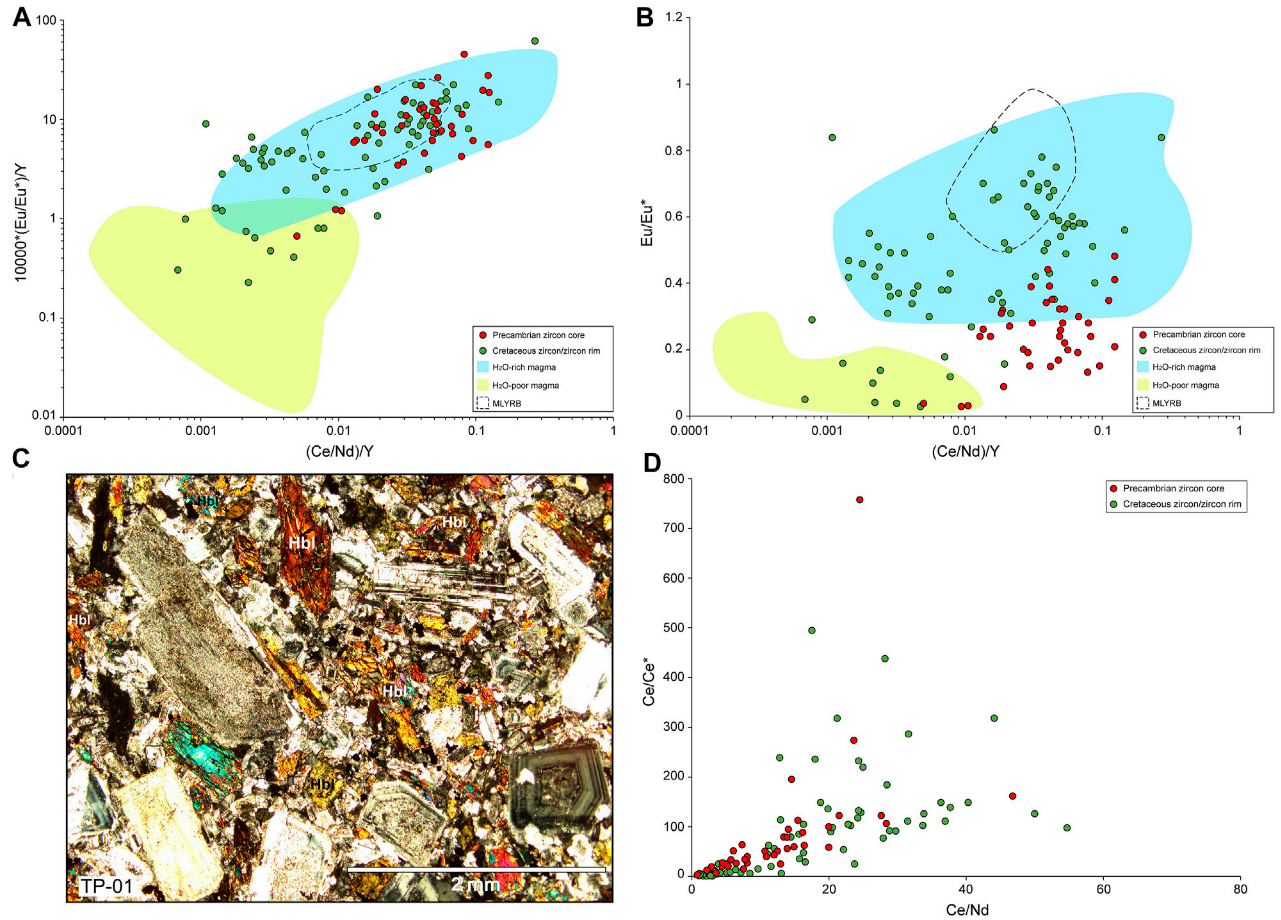

FIGURE 14 | (A) 10000*(Eu/Eu*)/Y vs. (Ce/Nd)/Y and **(B)** (Eu/Eu*)/Y vs. (Ce/Nd)/Y plots for zircons from the Huaibei-Linhuan intrusive rock samples (base map from Lu et al., 2016); **(C)** Thin-section microscopic photos showing the abundance of igneous hornblende in Taiping diorite (TP-01); **(D)** Zircon Ce/Ce* vs. Ce/Nd plot for the Huaibei-Linhuan intrusive rock samples, showing that Ce/Nd is a good proxy for Ce anomalies.

fluids (e.g., Mungall, 2002; Sillitoe, 2010; Zhang et al., 2017). Mungall et al. (2015) further proposed that sulfide liquids can ascend to the shallow crust through attaching with vapor bubbles, rather than only residing in the deep crust as traditionally believed. The reasons why the parental magma of the Huaibei-Linhuan adakites was particularly low-fO_2 (even lower than that of the ore-barren adakites along the southern Tanlu fault) is unclear, but may partly be attributed to the NCC lithospheric heterogeneity, especially along/near the southern Tanlu fault (e.g., Lü, 2019; Wang et al., 2020). In Huaibei-Linhuan, assimilation of the Carboniferous-Permian coal seams (as shown by the partially-assimilated natural coke fragments in our samples; **Figure 3**) would likely further reduce the fO_2 of the intruding dioritic-granodioritic magma, and hence further decrease its potential to form porphyry-style/-related Cu-Au mineralization.

CONCLUSIONS

1) Petrography, zircon U-Pb dating and whole-rock geochemistry suggests that the Huaibei-Linhuan intrusive rocks fall into two types, early-Early Cretaceous (ca. 130–129 Ma) high-Mg adakitic (quartz-)diorite and granodiorite, and late-Early Cretaceous (ca. 115.8 and 105.8 Ma) calc-alkaline microgabbro and dolerite.
2) The Huaibei-Linhuan high-Mg adakitic (quartz-)diorite and granodiorite are featured by low K_2O/Na_2O, high Sr/La, and lack of correlation between SiO_2 (fractionation index) and Sr/Y and MREE/HREE. This suggests that the adakites were not derived from high-pressure garnet-amphibole fractionation or partial melting of the thickened lower crust, but from partial melting of the subducted slab. Age correlation with the regional tectonic events suggests that the slab-melting may have caused by rollback of the subducting Paleo-Pacific slab instead. Further extension and crustal delamination along the southern Tanlu fault may have led to higher-degree partial melting (and lower-degree assimilation-fractionation) that formed the gabbro-dolerite in the Huaibei-Linhuan coalfield.
3) Parental magma of the Huaibei-Linhuan high-Mg adakites was considerably less oxidized than typical porphyry Cu-Au ore-forming magmas, although their water content may have been similarly high. The low magma fO_2 nature is supported

by both the low zircon Ce/Nd and whole-rock V/Sc ratios. The assimilation of the Carboniferous-Permian coal-bearing sequences in the area may have further decreased the magma fO_2, and thus its potential to form Cu-Au mineralization.

DATA AVAILABILITY STATEMENT

The original contributions presented in the study are included in the article/Supplementary Material, further inquiries can be directed to the corresponding author.

AUTHOR CONTRIBUTIONS

SZ: investigation, funding and writing. YA: supervision and writing. CL: data interpretation and writing. HW: analysis and academic support. YL: analysis and academic support. All authors have contributed to the article and approved the submitted version.

FUNDING

The project is jointly funded by the Natural Science Foundation of China (Grant No. 41802244) to the corresponding author.

ACKNOWLEDGMENTS

We sincerely thank Yuangao Sun, Shuai Zhang, and Qiang Fu for their field and logistic support. We would also like to thank Zhongqing Lin and Zheng Liu for assisting with the zircon U-Pb dating and whole-rock geochemical analysis. We are grateful to the Chief Editor Prof. David Lentz, the Handling Editor Prof. Hassan Mirnejad, and two knowledgeable reviewers for their insightful comments.

REFERENCES

Aeolus Lee, C.-T., Leeman, W. P., Canil, D., and Li, Z.-X. A. (2005). Similar V/Sc systematics in MORB and arc basalts: Implications for the oxygen fugacities of their mantle source regions. *J. Petrol.* 46, 2313–2336. doi:10.1093/petrology/egi056

An, Y., Liu, L., Wang, M., Zheng, S., Guo, Y., Zhang, S., et al. (2018). Source and enrichment of toxic elements in coal seams around mafic intrusions: Constraints from pyrites in the Yuandian Coal Mine in Anhui, Eastern China. *Minerals* 8 (4), 164. doi:10.3390/min8040164

Audétat, A., Pettke, T., Heinrich, C. A., and Bodnar, R. J. (2008). Special Paper: The Composition of Magmatic-Hydrothermal Fluids in Barren and Mineralized Intrusions. *Econ. Geology.* 103, 877–908. doi:10.2113/gsecongeo.103.5.877

Ballard, J. R., Palin, M. J., and Campbell, I. H. (2002). Relative oxidation states of magmas inferred from Ce(IV)/Ce(III) in zircon: Application to porphyry copper deposits of northern Chile. *Contrib. Mineral. Petrol.* 144, 347–364. doi:10.1007/s00410-002-0402-5

Barth, A. P., and Wooden, J. L. (2010). Coupled elemental and isotopic analyses of polygenetic zircons from granitic rocks by ion microprobe, with implications for melt evolution and the sources of granitic magmas. *Chem. Geology.* 277, 149–159. doi:10.1016/j.chemgeo.2010.07.017

Beate, B., Monzier, M., Spikings, R., Cotten, J., Silva, J., Bourdon, E., et al. (2001). Mio-Pliocene adakite generation related to flat subduction in southern Ecuador: the Quimsacocha volcanic center. *Earth Planet. Sci. Lett.* 192, 561–570. doi:10.1016/S0012-821X(01)00466-6

Belousova, E., Griffin, W., O'Reilly, S. Y., and Fisher, N. (2002). Igneous zircon: trace element composition as an indicator of source rock type. *Contrib. Mineral. Petrol.* 143, 602–622. doi:10.1007/s00410-002-0364-7

Castillo, P. R., Janney, P. E., and Solidum, R. U. (1999). Petrology and geochemistry of Camiguin Island, southern Philippines: Insights to the source of adakites and other lavas in a complex arc setting. *Contrib. Mineralogy Pet.* 134, 33–51. doi:10.1007/s004100050467

Chiaradia, M., Ulianov, A., Kouzmanov, K., and Beate, B. (2012). Why large porphyry Cu deposits like high Sr/Y magmas. *Sci. Repep* 2, 685. doi:10.1038/srep00685

Davidson, J., Turner, S., Handley, H., Macpherson, C., and Dosseto, A. (2007). Amphibole "sponge" in arc crust. *Geol* 35, 787–790. doi:10.1130/G23637A.110.1130/g23637a.1

Defant, M. J., and Drummond, M. S. (1993). Mount St. Helens: Potential example of the partial melting of the subducted lithosphere in a volcanic arc. *Geol* 21, 547–550. doi:10.1130/0091-7613(1993)021<0547:mshpeo>2.3.co;2

Deng, J., Yang, L.-Q., Groves, D. I., Zhang, L., Qiu, K.-F., and Wang, Q.-F. (2020). An integrated mineral system model for the gold deposits of the giant Jiaodong province, eastern China. *Earth-Science Rev.* 208, 103274. doi:10.1016/j.earscirev.2020.103274

Dilles, J. H., Kent, A. J. R., Wooden, J. L., Tosdal, R. M., Koleszar, A., Lee, R. G., et al. (2015). Zircon Compositional Evidence for Sulfur-degassing from Ore-forming Arc Magmas. *Econ. Geology.* 110, 241–251. doi:10.2113/econgeo.110.1.241

Dong, Y., Liu, J., Zhang, Y., Dou, S., Li, Y., Liu, S., et al. (2020). Early Cretaceous Xiuyan adakitic granitoids in the Liaodong Peninsula, eastern China: petrogenesis and implications for lithospheric thinning of the North China Craton. *Can. J. Earth Sci.* 58, 50–66. doi:10.1139/cjes-2020-0033

Goldfarb, R. J., and Santosh, M. (2014). The dilemma of the Jiaodong gold deposits: Are they unique. *Geosci. Front.* 5, 139–153. doi:10.1016/j.gsf.2013.11.00110.1016/j.gsf.2013.11.001

Gómez-Tuena, A., Langmuir, C. H., Goldstein, S. L., Straub, S. M., and Ortega-Gutiérrez, F. (2007). Geochemical evidence for slab melting in the trans-Mexican volcanic belt. *J. Petrol.* 48, 537–562. doi:10.1093/petrology/egl071

Grimes, C. B., Wooden, J. L., Cheadle, M. J., and John, B. E. (2015). "Fingerprinting" tectono-magmatic provenance using trace elements in igneous zircon. *Contrib. Mineral. Petrol.* 170, 46. doi:10.1007/s00410-015-1199-3

Hong, L., Xu, Y., Zhang, L., Liu, Z., Xia, X., and Kuang, Y. (2020). Oxidized Late Mesozoic subcontinental lithospheric mantle beneath the eastern North China Craton: A clue to understanding cratonic destruction. *Gondwana Res.* 81, 230–239. doi:10.1016/j.gr.2019.11.012

Hoskin, P. W. O., and Black, L. P. (2000). Metamorphic zircon formation by solid-state recrystallization of protolith igneous zircon. *J. Metamorphic Geology.* 18 (4), 423–439. doi:10.1046/j.1525-1314.2000.00266.x

Jiang, X.-Y., Deng, J.-H., Luo, J.-C., Zhang, L.-P., Luo, Z.-B., Yan, H.-B., et al. (2020). Petrogenesis of Early Cretaceous adakites in Tongguanshan Cu-Au polymetallic deposit, Tongling region, Eastern China. *Ore Geology. Rev.* 126, 103717. doi:10.1016/j.oregeorev.2020.103717

Jicha, B. R., and Singer, B. S. (2006). Volcanic history and magmatic evolution of Seguam Island, Aleutian Island arc, Alaska. *Geol. Soc. America Bull.* 118, 805–822. doi:10.1130/B2586110.1130/b25861.1

Kamvong, T., Khin Zaw, K., Meffre, S., Maas, R., Stein, H., and Lai, C.-K. (2014). Adakites in the Truong Son and Loei fold belts, Thailand and Laos: Genesis and implications for geodynamics and metallogeny. *Gondwana Res.* 26, 165–184. doi:10.1016/j.gr.2013.06.011

Li, C., Yan, J., Wang, A.-G., Liu, J.-M., and Li, Z.-S. (2020a). Petrogenesis of Cretaceous granitoids in the Bengbu-Wuhe area, southeastern North China Craton: Implications for gold mineralization. *Ore Geology. Rev.* 126, 103740. doi:10.1016/j.oregeorev.2020.103740

Li, J., Wang, K.-y., Cai, W.-y., Sun, F.-y., Liu, H.-l., Fu, L.-j., et al. (2020b). Triassic gold-silver metallogenesis in Qingchengzi orefield, North China Craton: Perspective from fluid inclusions, REE and H-O-S-Pb isotope systematics. *Ore Geology. Rev.* 121, 103567. doi:10.1016/j.oregeorev.2020.103567

Li, S., Jahn, B.-m., Zhao, S., Dai, L., Li, X., Suo, Y., et al. (2017). Triassic southeastward subduction of North China Block to South China Block: Insights from new geological, geophysical and geochemical data. *Earth-Science Rev.* 166, 270–285. doi:10.1016/j.earscirev.2017.01.009

Li, S., Zhao, G., Dai, L., Liu, X., Zhou, L., Santosh, M., et al. (2012). Mesozoic basins in eastern China and their bearing on the deconstruction of the North China Craton. *J. Asian Earth Sci.* 47, 64–79. doi:10.1016/j.jseaes.2011.06.008

Liu, J., Liu, F.-X., Li, S.-H., and Lai, C.-K. (2019). Formation of the Baiyun gold deposit, Liaodong gold province, NE China: Constraints from zircon U-Pb age, fluid inclusion, and C-H-O-Pb-He isotopes. *Ore Geol. Rev.*, 104. doi:10.1016/j.oregeorev.2018.12.006

Liu, J., Liu, F. X., Li, S. H., and Lai, C. K. (2020). Genesis of the Xiaotongjiapuzi gold deposit of the Liaodong gold province, Northeast China: Fluid inclusion thermometry and S-Pb-H-O-He isotope constraints. *Geol. J.* 55, 1023–1040. doi:10.1002/gj.3454

Liu, J., Ni, J., Chen, X., Craddock, J. P., Zheng, Y., Ji, L., et al. (2021). Early Cretaceous tectonics across the North Pacific: New insights from multiphase tectonic extension in Eastern Eurasia. *Earth-Science Rev.* 217, 103552. doi:10.1016/j.earscirev.2021.103552

Liu, S.-A., Li, S., Guo, S., Hou, Z., and He, Y. (2012). The Cretaceous adakitic-basaltic-granitic magma sequence on south-eastern margin of the North China Craton: Implications for lithospheric thinning mechanism. *Lithos* 134-135 (135), 163–178. doi:10.1016/j.lithos.2011.12.015

Liu, S.-A., Li, S., He, Y., and Huang, F. (2010a). Geochemical contrasts between early Cretaceous ore-bearing and ore-barren high-Mg adakites in central-eastern China: Implications for petrogenesis and Cu-Au mineralization. *Geochimica et Cosmochimica Acta* 74, 7160–7178. doi:10.1016/j.gca.2010.09.003

Liu, Y., Gao, S., Hu, Z., Gao, C., Zong, K., and Wang, D. (2010b). Continental and Oceanic Crust Recycling-induced Melt-Peridotite Interactions in the Trans-North China Orogen: U-Pb Dating, Hf Isotopes and Trace Elements in Zircons from Mantle Xenoliths. *J. Pet.* 51, 537–571. doi:10.1093/petrology/egp082

Liu, Y., Hu, Z., Gao, S., Günther, D., Xu, J., Gao, C., et al. (2008). *In situ* analysis of major and trace elements of anhydrous minerals by LA-ICP-MS without applying an internal standard. *Chem. Geology.* 257, 34–43. doi:10.1016/j.chemgeo.2008.08.004

Loucks, R. R., Fiorentini, M. L., and Henríquez, G. J. (2020). New Magmatic Oxybarometer Using Trace Elements in Zircon. *J. Petrol.*, 61. doi:10.1093/petrology/egaa034

Lü, Q., Meng, G., Zhang, K., Liu, Z., Yan, J., Shi, D., et al. (2021). The lithospheric architecture of the Lower Yangtze Metallogenic Belt, East China: Insights into an extensive Fe-Cu mineral system. *Ore Geology. Rev.* 132, 103989. doi:10.1016/j.oregeorev.2021.103989

Lu, Y.-J., Loucks, R. R., Fiorentini, M., McCuaig, T. C., Evans, N. J., Yang, Z.-M., et al. (2016). Zircon Compositions as a Pathfinder for Porphyry Cu ± Mo ± Au Deposits. *Tectonics Metallog. Tethyan Orog. Belt* 19, 0. doi:10.5382/SP.19.13

Lü, Z. (2019). Uppermost mantle velocity and anisotropy structure beneath the North China Craton and its adjacent regions. *Tectonophysics* 754, 45–55. doi:10.1016/j.tecto.2019.01.014

Ludwig, K. R. (2003). *ISOPLOT 3.00: A Geochronological Toolkit for Microsoft Excel.* Berkeley: Berkeley Geochronology CenterCalifornia.

Macpherson, C. G. (2008). Lithosphere erosion and crustal growth in subduction zones: Insights from initiation of the nascent East Philippine Arc. *Geol* 36, 311–314. doi:10.1130/G24412A.1

Maniar, P. D., and Piccoli, P. M. (1989). Tectonic discrimination of granitoids. *Geol. Soc. Am. Bull.* 101 (5), 635–643. doi:10.1130/0016-7606(1989)101<0635:tdog>2.3.co;2

Mao, J., Wang, Y., Lehmann, B., Yu, J., Du, A., Mei, Y., et al. (2006). Molybdenite Re-Os and albite 40Ar/39Ar dating of Cu-Au-Mo and magnetite porphyry systems in the Yangtze River valley and metallogenic implications. *Ore Geology. Rev.* 29, 307–324. doi:10.1016/j.oregeorev.2005.11.001

Middlemost, E. A. K. (1994). Naming materials in the magma/igneous rock system. *Earth-Science Rev.* 37, 215–224. doi:10.1016/0012–8252(94)90029–9

Mori, L., Gómez-Tuena, A., Cai, Y., and Goldstein, S. L. (2007). Effects of prolonged flat subduction on the Miocene magmatic record of the central Trans-Mexican Volcanic Belt. *Chem. Geology.* 244, 452–473. doi:10.1016/j.chemgeo.2007.07.002

Mungall, J. E., Brenan, J. M., Godel, B., Barnes, S. J., and Gaillard, F. (2015). Transport of metals and sulphur in magmas by flotation of sulphide melt on vapour bubbles. *Nat. Geosci* 8, 216–219. doi:10.1038/ngeo2373

Mungall, J. E. (2002). Roasting the mantle: Slab melting and the genesis of major Au and Au-rich Cu deposits. *Geol* 30, 915–918. doi:10.1130/0091-7613(2002)030<0915:rtmsma>2.0.co;2

Pearce, J. (1996). A user's Guide to basalt discrimination diagrams. *Geol. Assoc. Can. Short Course Notes* 12, 79–113. doi:10.1111/j.1438–8677.1980.tb03374.x10.1093/oq/12.3.83

Peccerillo, A., and Taylor, S. R. (1976). Geochemistry of Eocene Calc-Alkaline Volcanic Rocks from the Kastamonu Area, Northern Turkey. *Contr. Mineral. Petrol.* 58, 63–81. doi:10.1007/BF00384745

Ping, X., Zheng, J., Xiong, Q., Griffin, W. L., Yu, C., and Su, Y. (2019). Downward rejuvenation of the continental lower crust beneath the southeastern North China Craton. *Tectonophysics* 750, 213–228. doi:10.1016/j.tecto.2018.11.012

Pirajno, F., and Zhou, T. (2015). Intracontinental Porphyry and Porphyry-Skarn Mineral Systems in Eastern China: Scrutiny of a Special Case "Made-in-China". *Econ. Geology.* 110, 603–629. doi:10.2113/econgeo.110.3.603

Reich, M., Parada, M. A., Palacios, C., Dietrich, A., Schultz, F., and Lehmann, B. (2003). Adakite-like signature of Late Miocene intrusions at the Los Pelambres giant porphyry copper deposit in the Andes of central Chile: metallogenic implications. *Mineralium Deposita* 38, 876–885. doi:10.1007/s00126–003–0369–9

Reubi, O., and Nicholls, I. A. (2004). Magmatic evolution at Batur volcanic field, Bali, Indonesia: petrological evidence for polybaric fractional crystallization and implications for caldera-forming eruptions. *J. Volcanology Geothermal Res.* 138, 345–369. doi:10.1016/j.jvolgeores.2004.07.009

Richards, J. P. (2011). High Sr/Y Arc Magmas And Porphyry Cu Mo Au Deposits: Just Add Water. *Econ. Geology.* 106, 1075–1081. doi:10.2113/econgeo.106.7.1075

Richards, J. P., and Kerrich, R. (2007). Special Paper: Adakite-Like Rocks: Their Diverse Origins and Questionable Role in Metallogenesis. *Econ. Geology.* 102 (4), 537–576. doi:10.2113/gsecongeo.102.4.537

Richards, J. P., Spell, T., Rameh, E., Razique, A., and Fletcher, T. (2012). High Sr/Y Magmas Reflect Arc Maturity, High Magmatic Water Content, and Porphyry Cu ± Mo ± Au Potential: Examples from the Tethyan Arcs of Central and Eastern Iran and Western Pakistan. *Econ. Geol.* 107, 295–332. doi:10.2113/econgeo.107.2.295

Sillitoe, R. H. (2010). Porphyry copper systems. *Econ. Geology.* 105, 3–41. doi:10.2113/gsecongeo.105.1.3

Sun, P., Guo, P., and Niu, Y. (2021). Eastern China continental lithosphere thinning is a consequence of paleo-Pacific plate subduction: A review and new perspectives. *Earth-Science Rev.* 218, 103680. doi:10.1016/j.earscirev.2021.103680

Sun, S.-s., and McDonough, W. F. (1989). Chemical and isotopic systematics of oceanic basalts: implications for mantle composition and processes. *Geol. Soc. Lond. Spec. Publications* 42, 313–345. doi:10.1144/GSL.SP.1989.042.01.19

Sun, W., Xie, Z., Chen, J., and Zhang, X. (2003). Os-Os dating of copper and molybdenum deposits along the Middle and Lower reaches of the Yangtze River, China. *Econ. Geology.* 98, 175–180. 0361–0128/01/3323/175–610.2113/98.1.175.

Wang, K., Chen, L., Xiong, X., Yan, Z., and Xie, R. (2020). The role of lithospheric heterogeneities in continental rifting: Implications for rift diversity in the North China Craton. *J. Geodynamics* 139, 101765. doi:10.1016/j.jog.2020.101765

Wang, Q., Xu, J.-F., Jian, P., Bao, Z.-W., Zhao, Z.-H., Li, C.-F., et al. (2006). Petrogenesis of Adakitic Porphyries in an Extensional Tectonic Setting, Dexing, South China: Implications for the Genesis of Porphyry Copper Mineralization. *J. Petrol.* 47, 119–144. doi:10.1093/petrology/egi070

Xia, Q.-K., Hao, Y.-T., Liu, S.-C., Gu, X.-Y., and Feng, M. (2013). Water contents of the Cenozoic lithospheric mantle beneath the western part of the North China Craton: Peridotite xenolith constraints. *Gondwana Res.* 23 (1), 108–118. doi:10.1016/j.gr.2012.01.010

Xie, G.-Q., Mao, J.-W., Li, R.-L., Qü, W.-J., Pirajno, F., and Du, A.-D. (2007). Re-Os molybdenite and Ar-Ar phlogopite dating of Cu-Fe-Au-Mo (W) deposits in southeastern Hubei, China. *Mineralogy Pet.* 90, 249–270. doi:10.1007/s00710–006–0176–y

Xu, W.-L., Gao, S., Yang, D.-B., Pei, F.-P., and Wang, Q.-H. (2009). Geochemistry of eclogite xenoliths in Mesozoic adakitic rocks from Xuzhou-Suzhou area in central China and their tectonic implications. *Lithos* 107 (3), 269–280. doi:10.1016/j.lithos.2008.11.004

Xu, W., Gao, S., Wang, Q., Wang, D., and Liu, Y. (2006). Mesozoic crustal thickening of the eastern North China craton: Evidence from eclogite xenoliths and petrologic implications. *Geol* 34 (9), 721–724. doi:10.1130/G22551.1

Xu, W. L., Wang, Q. H., Liu, X. C., Wang, D. Y., and Guo, J. H. (2004). Chronology and Sources of Mesozoic Intrusive Complexes in the Xuzhou-Huainan Region, Central China: Constraints from SHRIMP Zircon U-Pb Dating. *Acta Geologica Sinica (English Edition)* 78 (1), 96–106. doi:10.1111/j.1755–6724.2004.tb00679.x

Xu, Y.-M., Jiang, S.-Y., and Zhu, J.-X. (2021). Factors controlling the formation of large porphyry Cu deposits: A case study from the Jiurui ore district of Middle-Lower Yangtze River Metallogenic Belt using *in situ* zircon and apatite chemistry from syn-mineralization intrusions. *Ore Geology. Rev.* 133, 104082. doi:10.1016/j.oregeorev.2021.104082

Yang, D.-B., Xu, W.-L., Wang, Q.-H., and Pei, F.-P. (2010). Chronology and geochemistry of Mesozoic granitoids in the Bengbu area, central China: Constraints on the tectonic evolution of the eastern North China Craton. *Lithos* 114 (1-2), 200–216. doi:10.1016/j.lithos.2009.08.009

Yang, J.-H., Wu, F.-Y., Wilde, S. A., Belousova, E., and Griffin, W. L. (2008). Mesozoic decratonization of the North China block. *Geol* 36 (6), 467–470. doi:10.1130/G24518A.1

Yangliu Coal Industry Co. Ltd (2017). Resources verification report on the reserves of Yangliu Coal Mine in Suixi County, Anhui Province. *Huaibei, Anhui*, 62–65.

Yao, Y., and Liu, D. (2012). Effects of igneous intrusions on coal petrology, pore-fracture and coalbed methane characteristics in Hongyang, Handan and Huaibei coalfields, North China. *Int. J. Coal Geology.* 96-97, 72–81. doi:10.1016/j.coal.2012.03.007

Ye, G., Liu, C., Luo, X., Jin, S., Wei, W., Dong, H., et al. (2021). Dynamical significance of the Tanlu Fault Zone in the destruction of the North China Craton: The evidence provided by the three-dimensional Magnetotelluric array study. *Tectonophysics* 813, 228910. doi:10.1016/j.tecto.2021.228910

Zhang, C.-c., Sun, W.-d., Wang, J.-t., Zhang, L.-p., Sun, S.-j., and Wu, K. (2017). Oxygen fugacity and porphyry mineralization: A zircon perspective of Dexing porphyry Cu deposit, China. *Geochimica et Cosmochimica Acta* 206, 343–363. doi:10.1016/j.gca.2017.03.013

Zhang, C., Ma, C., Holtz, F., Koepke, J., Wolff, P. E., and Berndt, J. (2013). Mineralogical and geochemical constraints on contribution of magma mixing and fractional crystallization to high-Mg adakite-like diorites in eastern Dabie orogen, East China. *Lithos* 172-173, 118–138. doi:10.1016/j.lithos.2013.04.011

Zhang, J., Qu, J., Zhang, B., Zhao, H., Niu, P., Zhao, S., et al. (2020). Mesozoic intraplate deformation of the central North China Craton: Mechanism and tectonic setting. *J. Asian Earth Sci.* 192, 104269. doi:10.1016/j.jseaes.2020.104269

Zhang, Y., Cheng, J., Tian, J., Pan, J., Sun, S., Zhang, L., et al. (2019a). Texture and trace element geochemistry of quartz in skarn system: Perspective from Jiguanzui Cu-Au skarn deposit, Eastern China. *Ore Geol. Rev.*, 109. doi:10.1016/j.oregeorev.2019.05.007

Zhang, Z., Wang, Y., Li, D., and Lai, C. (2019b). Lithospheric architecture and metallogenesis in Liaodong peninsula, North China Craton: Insights from zircon Hf-Nd isotope mapping. *Minerals* 9, 179. doi:10.3390/min9030179

Zhao, L., Allen, R. M., Zheng, T., and Hung, S.-H. (2009). Reactivation of an Archean craton: Constraints from P- and S-wave tomography in North China. *Geophys. Res. Lett.* 36 (17), 367–389. doi:10.1029/2009GL039781

Zhao, M., An, Y., Wang, M., Ding, M., and Lai, C. (2019). New Genesis of Natural Coke around Magmatic Intrusion at the Shitai Coalmine of Huaibei City, North China. *Acta Geologica Sinica - English Edition* 93 (4), 1158–1159. doi:10.1111/1755-6724.13827

Zhao, T., Zhu, G., Lin, S., and Wang, H. (2016). Indentation-induced tearing of a subducting continent: Evidence from the Tan-Lu Fault Zone, East China. *Earth-Science Rev.* 152, 14–36. doi:10.1016/j.earscirev.2015.11.003

Zhao, Z., Liang, S., Santosh, M., and Wei, J. (2020). Lithospheric extension associated with slab rollback: Insights from early Cretaceous magmatism in the southern segment of Tan-Lu fault zone, central-eastern China. *Lithos* 362-363, 105487. doi:10.1016/j.lithos.2020.105487

Zhou, H., Shang, D. F., Chan, S. W., and Chen, J. (2019). Zircon U-Pb dating, petrogenesis and geological significance of the Banjing pluton in Xuhuai area. *J. Mineral. Petrol.* 39, 9–16. (in Chinese with English abstract).

Zhou, T., Wang, S., Fan, Y., Yuan, F., Zhang, D., and White, N. C. (2015). A review of the intracontinental porphyry deposits in the Middle-Lower Yangtze River Valley metallogenic belt, Eastern China. *Ore Geology. Rev.* 65, 433–456. doi:10.1016/j.oregeorev.2014.10.002

Zhu, G., Liu, G. S., Niu, M. L., Xie, C. L., Wang, Y. S., and Xiang, B. (2009). Syn-collisional transform faulting of the Tan-Lu fault zone, East China. *Int. J. Earth Sci. (Geol Rundsch)* 98, 135–155. doi:10.1007/s00531–007–0225–8

Zhu, G., Wang, Y., Liu, G., Niu, M., Xie, C., and Li, C. (2005). 40Ar/39Ar dating of strike-slip motion on the Tan-Lu fault zone, East China. *J. Struct. Geology.* 27, 1379–1398. doi:10.1016/j.jsg.2005.04.007

Conflict of Interest: The authors declare that the research was conducted in the absence of any commercial or financial relationships that could be construed as a potential conflict of interest.

Publisher's Note: All claims expressed in this article are solely those of the authors and do not necessarily represent those of their affiliated organizations, or those of the publisher, the editors and the reviewers. Any product that may be evaluated in this article, or claim that may be made by its manufacturer, is not guaranteed or endorsed by the publisher.